The conserved molting/circadian rhythm regulator NHR-23/NR1F1 serves as an essential co-regulator of *C. elegans* spermatogenesis

James Matthew Ragle[1], Abigail L. Aita[2], Kayleigh N. Morrison[2], Raquel Martinez-Mendez[1], Hannah N. Saeger[1], Guinevere A. Ashley[1], Londen C. Johnson[1], Katherine A. Schubert[1], Diane C. Shakes[2], and Jordan D. Ward[1,‡].

[1]Department of Molecular, Cell, and Developmental Biology, University of California-Santa Cruz, Santa Cruz, CA 95064, USA.

[2]Department of Biology, William & Mary, Williamsburg, VA 23187, USA.

[‡]Author for correspondence.

Corresponding author email: jward2@ucsc.edu

Keywords: *C. elegans*, spermatogenesis, NHR-23, nuclear hormone receptor, meiosis, auxin-inducible degron

Summary Statement

A well-characterized regulator of *C. elegans* molting also unexpectedly controls the spermatogenesis program; our work provides insights into the gene regulatory networks controlling spermatogenesis.

Abstract

In sexually reproducing metazoans, spermatogenesis is the process by which uncommitted germ cells give rise to haploid sperm. Work in model systems has revealed mechanisms controlling commitment to the sperm fate, but how this fate is subsequently executed remains less clear. While studying the well-established role of the conserved nuclear hormone receptor transcription factor, NHR-23/NR1F1, in regulating *C. elegans* molting, we discovered NHR-23/NR1F1 is also constitutively expressed in developing 1^0 spermatocytes and is a critical regulator of spermatogenesis. In this novel role, NHR-23/NR1F1 functions downstream of the canonical sex determination pathway. Degron-mediated depletion of NHR-23/NR1F1 within hermaphrodite or male germlines causes sterility due to an absence of functional sperm as depleted animals produce arrested primary spermatocytes rather than haploid sperm. These spermatocytes arrest in prometaphase I and fail to either progress to anaphase or attempt spermatid-residual body partitioning. They make sperm-specific membranous organelles (MOs) but fail to assemble their major sperm protein into fibrous bodies. NHR-23/NR1F1 appears to function independently of the known SPE-44 gene regulatory network, revealing the existence of an NHR-23/NR1F1-mediated module that regulates the spermatogenesis program.

Introduction

Transcription factors perform diverse roles in the development of specialized cell types. Many work synergistically in gene regulatory networks to execute complex programs of cell differentiation (Drapek et al., 2017; Levine and Davidson, 2005; Medwig-Kinney et al., 2020). These networks coordinate the expression of enzymes, modifiers, and structural proteins that characterize a specific cell type. One challenge of studying transcription factors is they often function with distinct co-regulators in multiple developmental contexts. For example in the nematode *Caenorhabditis elegans*, the GATA-1 transcription factor ELT-1 is essential for epidermal cell fates during embryogenesis (Page et al., 1997) but later regulates the expression of multiple sperm genes (del Castillo-Olivares et al., 2009). In knockout or null mutants, if disruption of the first developmental event results in embryonic or larval lethality, later functions will be missed. Traditionally this challenge has been addressed using conditional mutants, mRNA depletion by RNA interference, or genetic mosaics. A powerful new addition to this investigational toolbox is the auxin-inducible degron (AID) system for the conditional disruption of protein function (Nishimura et al., 2009; Zhang et al., 2015). In this system, a gene of interest tagged with an AID sequence is co-expressed with a TIR1 F-box protein driven by a tissue-specific promoter. In the presence of the plant hormone, auxin, the TIR1 containing E3 ubiquitin ligase polyubiquitinates the AID sequence, leading to degradation of the AID-tagged protein. This conditional protein depletion system is ideal for characterizing the distinct functions of an essential, multi-functional transcription factor.

One motivation of developing the AID system in *C. elegans* was to study events in meiosis required for gametogenesis (Zhang et al., 2015). During gametogenesis, stem cell precursors enact a developmental program producing highly specialized haploid sperm or oocytes. *C. elegans* is a powerful model to study gametogenesis as hermaphrodites produce a limited number of sperm before switching exclusively to producing oocytes whereas males produce sperm continuously (Ellis and Schedl, 2007)(Fig. 1A,B). Extensive studies of *C. elegans* sex determination (Barton and Kimble, 1990; Ellis and Schedl, 2007) identified the transcription factor TRA-1, a homolog of GLI and cubitus interruptus, as the key regulator of somatic sex determination and the spermatocyte/oocyte decision (Hodgkin, 1987; Schedl et al.,

1989; Zarkower and Hodgkin, 1992). Within the germline, TRA-1 promotes oogenesis/inhibits spermatogenesis by repressing expression of two germline-specific, RNA-binding proteins (FOG-1 and FOG-3)(Chen and Ellis, 2000; Jin et al., 2001). A different RNA-binding translational repressor, PUF-8, maintains sperm fate (Subramaniam and Seydoux, 2003).

Beyond the initial sperm fate decision, the subsequent control of sperm differentiation remains poorly understood. Understanding the gene networks that regulate sperm differentiation offers an inroad into this question. Many *C. elegans* germline genes primarily rely on mRNA 3' untranslated regions (UTRs), not promoters, to ensure expression at the correct time and location during germline development (Merritt et al., 2008). In contrast, spermatocyte promoters provide spatiotemporal control of gene expression, making transcription factors direct regulators of sperm differentiation (Merritt et al., 2008). The *C. elegans* transcription factor SPE-44 is widely distributed on autosomes of developing spermatocytes and directly regulates other transcription factors like *elt-1* as well as sperm function genes such as kinases and structural components (Kulkarni et al., 2012). Which other transcription factors contribute to gene expression regulation in *C. elegans* spermatogenesis and to what degree they control similar or disparate sets of genes remains unknown.

Spermatogenesis is a complex cellular process involving a host of dynamic subcellular events coordinated by a large number of genes. Because of its linear organization, the full developmental sequence of spermatogenesis can be analyzed in individual gonads (Fig. 1C, Chu and Shakes, 2013). Undifferentiated germ cells proliferate mitotically at the distal end while mature primary spermatocytes divide meiotically at the proximal end (Fig. 1C,D). The commitment to sperm fate occurs as undifferentiated germ cells exit mitosis and initiate meiotic homolog pairing. Transcription of spermatogenesis genes and translation of most sperm proteins occurs within an extended pachytene zone. During the subsequent karyosome stage, global transcription ceases as chromosomes detach from the nuclear envelope and coalesce into a central mass (Shakes et al., 2009). Although transcription stops, translation and assembly of sperm-specific complexes continue (Chu and Shakes, 2013; Shakes et al., 2009). Throughout meiotic prophase, each individual spermatocyte is linked to a shared central rachis via a syncytial connection (Fig. 1D). Following the karyosome stage,

primary spermatocytes detach from the rachis before undergoing the meiotic divisions. Post-meiotic development is limited to a post-meiotic partitioning event in which spermatids separate from a central residual body and the spherical spermatids activating to acquire motility through extension of a pseudopod (Chu and Shakes, 2013; Ward et al., 1981). Despite having large collections of mutants affecting the processes of sperm differentiation (Nishimura and L'Hernault, 2010), how these events are coordinated is not well-understood.

C. elegans NHR-23/NR1F1 (hereafter referred to as NHR-23) is a nuclear hormone receptor (NHR) transcription factor previously shown to be involved in embryonic epidermal development (Kostrouchova et al., 1998), larval molting (Kostrouchova et al., 1998; Kostrouchova et al., 2001), and diet-induced developmental acceleration (Macneil et al., 2013). The mammalian orthologs (RORs/NR1F) regulate circadian rhythms (Akashi and Takumi, 2005; André et al., 1998; Sato et al., 2004), and the insect ortholog (DHR3) regulates metamorphosis (Kageyama et al., 1997; Lam et al., 1997; White et al., 1997). Loss or reduction of *nhr-23* activity leads to embryonic lethality, larval arrest, or larval lethality (Kostrouchova et al., 1998; Kostrouchova et al., 2001; Kouns et al., 2011). Lethality following *nhr-23* inactivation occurs early in development, masking an unanticipated later role for NHR-23 in spermatogenesis which we describe here. Our results are the first to show that *nhr-23* is expressed within developing spermatocytes and functions downstream of the canonical sex determination pathway. Depletion of NHR-23 protein results in sperm-specific sterility. Affected spermatocytes arrest in meiosis I prometaphase and exhibit developmental defects in biogenesis of an essential sperm-specific organelle. NHR-23 promotes spermatogenesis in a distinct pathway from SPE-44. Our work provides new insights into how transcription factors coordinately execute the spermatogenesis program.

Results

NHR-23:GFP is expressed in sperm-producing germlines

To explore potential functions of NHR-23 beyond molting, we wanted to know where and when NHR-23 is expressed. To address this question, we used CRISPR/Cas9-mediated genome editing to introduce a multifunctional GFP::AID*::3xFLAG

sequence into the endogenous *nhr-23* locus, tagging all known isoforms. AID* is a minimal, 44 amino acid auxin-inducible degron sequence. Consistent with previous promoter reporters and immunolabelling (Kostrouchova et al., 1998), NHR-23::GFP expression was observed in epidermal cell nuclei of 1.5-stage embryos and in hypodermal and seam cells of developing larvae (unpublished data). Somatic cell expression persisted in L4 larvae, specifically in hypodermal cells of the head, vulval precursor cells of hermaphrodites, and hypodermal and tail cells of males (Fig. 2A). Notably, NHR-23::GFP was also expressed in the sperm-producing germlines of males and L4 hermaphrodites, but not in hermaphrodites only producing oocytes (Fig. 2B). Previous studies missed this spermatocyte expression as transgenes are frequently silenced in the germline and immunolabelling was limited to embryos (Kostrouchova et al., 1998; Kostrouchova et al., 2001).

In males (and sperm-producing hermaphrodites), NHR-23::GFP was first observed in early pachytene spermatocytes (Fig. 2C), increased in intensity through late pachytene (Fig. 2B, C), and became undetectable during late meiotic prophase with onset of chromatin condensation (Fig. 2D). NHR-23 was undetectable in meiotically dividing spermatocytes or mature spermatids. This overall pattern is similar to that reported for SPE-44 (Kulkarni et al., 2012). Also like SPE-44, NHR-23::GFP labeled most chromosomes along their entire length yet failed to label a portion of DNA in each pachytene stage spermatocyte (Fig. 2E). Presumably NHR-23 is not labelling the X chromosome, which is transcriptionally silent during spermatocyte meiosis (Kelly et al., 2002).

Auxin-induced NHR-23-depletion during or before spermatogenesis causes infertility in males and hermaphrodites

Because both *nhr-23* null mutants and RNAi knockdowns of L1 larvae arrest as early larvae (Kostrouchova et al., 1998; Kostrouchova et al., 2001), previous studies failed to assess potential NHR-23 functions in the germline. Conversely, RNAi treatment of L3/L4 hermaphrodites or adult males failed to detectably deplete NHR-23 in the germline (unpublished data). We therefore turned to auxin-inducible degradation (Nishimura et al., 2009; Zhang et al., 2015), which allows for tissue-specific, temporally regulated depletion of proteins. Our multifunctional NHR-23 knock-in construct contained the AID* sequence necessary for auxin- and TIR-dependent

depletion of target proteins. A separate TIR1 transgene included the strong *mex-5* promoter (Schubert et al., 2000) which would allow NHR-23-depletion primarily in the germline. Hermaphrodites expressing either *mex-5::TIR1* or *nhr-23::GFP::AID*::3xFLAG* grew to adulthood and were fully fertile whether grown on control or 4 mM auxin media (Fig. 3A). Hermaphrodites expressing both constructs were fully fertile on control media but produced no progeny when grown on media with 4 mM auxin. Crossing NHR-23-depleted hermaphrodites to wild type males restored fertility (Fig. 3B). These results suggest NHR-23 is necessary for sperm production in hermaphrodites.

We next carried out a set of experiments to determine when during development NHR-23 is necessary for fertility. Synchronized *mex-5::TIR, nhr-23::GFP::AID*::3xFLAG* hermaphrodites were placed on control or 4 mM auxin media (Fig. 3C). Hermaphrodites were shifted from control media to auxin, or vice versa. A short auxin exposure early in larval development (L1-L2) or continuous exposure after young adulthood had little or no effect on hermaphrodite self-fertility. The auxin-sensitive period was the L4 larval stage, with auxin exposure causing partially penetrant or complete self-infertility. Self-infertility was more pronounced in "shift-off" treatments, presumably due to the reported slow recovery of AID-tagged proteins following auxin removal (Zhang et al., 2015). Western blotting experiments revealed ~70% depletion of NHR-23 (Fig. 3D, Fig. S2). Since we specifically depleted NHR-23::GFP in the germline in adult males, it is possible that somatic expression below the detection threshold of our fluorescent imaging contributes to the residual NHR-23::GFP detected following auxin treatment.

While spermatogenesis is similar in *C. elegans* males and hermaphrodites, sex-specific differences do exist (L'Hernault et al., 1988; Minniti et al., 1996; Nance et al., 1999; Nance et al., 2000; Shakes and Ward, 1989). To test whether NHR-23 also functioned in male spermatogenesis, we repeated the crossing experiment from Fig. 3B using *mex-5::TIR1, nhr-23::GFP::AID*::3xFLAG* males. Males grown on control media sired progeny when crossed to either NHR-23-depleted hermaphrodites or feminized but otherwise wildtype *fog-1* "females", but males grown on 4 mM auxin did not sire any progeny (Fig. 3B). We confirmed that NHR-23-depleted males were mating both by observation and assessing the transfer of seminal fluid while mating with *spe-8*

hermaphrodites (Shakes and Ward, 1989)(Fig. S3). Sperm activation defects preclude self-fertility in *spe-8* hermaphrodites, but their sperm can be transactivated by male seminal fluid. Non-celibate, NHR-23-depleted adult males mated with *spe-8* hermaphrodites produced no outcross progeny, but some matings induced *spe-8* self-progeny. Unexpectedly, some crosses set up with L4 males yielded both self and outcross progeny, suggesting that incomplete NHR-23 degradation allows the early production of functional sperm.

NHR-23 acts following the sperm/oocyte decision

The infertility phenotype could suggest that NHR-23 was either a spermatocyte/oocyte cell fate determinant or responsible for executing the sperm fate program. To place NHR-23 in relation to known sex determination factors (Ellis and Schedl, 2007), we performed epistasis experiments (Fig. 4A). We crossed *nhr-23::GFP::AID*::3xFLAG* into a temperature sensitive (ts) gain-of-function *fem-3(q20)* allele genetic background (Barton et al., 1987). At 15°C, hermaphrodites produce both sperm and oocytes, and NHR-23 expression was limited to the L4 stage (Fig. 4B). At 25°C, the masculinized germline produced only sperm, and NHR-23 expression persisted throughout adulthood. These results indicate that NHR-23 functions downstream of FEM-3. Next, we tested *fog-3 (feminization of germline*), which along with *fog-1* is believed to act as the terminal, germline-specific selector for sperm fate. As *fog-3* is close to *nhr-23* on chromosome I, we directly engineered a putative null allele of *fog-3* in an *nhr-23::GFP::BioTag::AID*::3xFLAG* strain (*wrd1* allele) by introducing a premature termination codon followed by a frameshift at the *fog-3* locus (*wrd6* allele*)*. Because this experiment utilized a *nhr-23* strain distinct from the *wrd8* allele used elsewhere in this study, we verified that germline-specific NHR-23-depletion in a *sun-1p::TIR1; nhr-23(wrd1[GFP::BioTag::AID*::3xFLAG])* strain also caused sterility (Fig. S1). Importantly, this result demonstrates an equivalent phenotype with two distinct AID*-tagged *nhr-23* alleles and TIR1 transgenes being driven by two different germline-specific promoters (*mex-5p* vs *sun-1p)* (Fig. 3A; Fig. S2). In *fog-3(wrd6)* heterozygotes, NHR-23::GFP was expressed specifically in L4 hermaphrodites (Fig. 4C). In *fog-3(wrd6)* homozygotes, germline feminization is accompanied by a complete loss of NHR-23::GFP expression in L4 animals. These results show NHR-23 operates downstream of the known sex determination pathway, after spermatocyte cell fate has been decided.

Germline depletion of NHR-23 results in spermatocyte arrest

To better understand the nature of sperm-related fertility defects, we used DIC optics to examine gonads of control and NHR-23-depleted animals. The proximal gonad of control males contained a linear sequence of (1) spermatocytes completing meiotic prophase, (2) a discrete zone of meiotically dividing spermatocytes, budding figures, and residual bodies, and finally, (3) a zone of tightly packed spermatids with their small, highly refractive chromatin mass (Figs. 1B, 5A). NHR-23-depleted germlines produced spermatocytes that progressed normally through meiotic prophase. However, the rest of the gonad filled with what appeared to be primary spermatocytes. Haploid spermatids were notably absent. Depletion of NHR-23 in masculinized germlines of *fbf-1(ok91) fbf-2(q704)* hermaphrodites yielded similar defects (Fig. 5B), indicating NHR-23-depletion during either male or hermaphrodite spermatogenesis results in a spermatocyte arrest phenotype.

To independently confirm our NHR-23 depletion results, we depleted *nhr-23* mRNA in the germline using transgene-mediated co-suppression, which is similar to RNAi (Dernburg et al., 2000). This method yielded viable but infertile male animals with the same spermatogenesis defects as their auxin-mediated depletion counterparts, confirming the phenotypes are due to NHR-23-depletion (Fig. 5C).

NHR-23-depleted primary spermatocytes arrest in a metaphase I-like state

To determine which stages of spermatogenesis are affected by NHR-23 depletion, we assessed nuclear morphology in male germlines. Hoechst staining of DNA in control male germlines revealed the expected stages: i) diakinesis stage (Diak) spermatocytes with intact nuclear envelopes; ii) meiotically dividing spermatocytes; and iii) cells undergoing the post-meiotic partitioning (Par) event that yields a central residual body (RB) and four haploid spermatids (S) (Fig. 1, Fig. 6A). NHR-23-depleted male germlines included diakinesis spermatocytes and spermatocytes with chromosome patterns suggesting they were arresting in prometaphase or metaphase I (Fig. 6B). Notably, these germlines lacked secondary spermatocytes, budding figures, or spermatids (Figs. 1D, 6B). In many cells, chromosomes were spread out relative to the initial metaphase clusters (Fig. 6B, early arrest), but there was no evidence of actual

anaphase chromosome segregation. Nuclear envelope breakdown was independently confirmed by labelling fixed gonads with nuclear pore antibodies (Fig. 6I,J, unpublished data). These data suggested that spermatocyte development was aberrant, with an arrest in prometaphase or metaphase I.

To determine how well NHR-23-depleted spermatocytes were entering or exiting M-phase, isolated male gonads were first co-labelled with DAPI, anti-tubulin and anti-phospho-histone H3 Serine 10 (pHisH3(ser10)), a proxy for activity of the cell cycle regulator Aurora kinase (Hsu et al., 2000)(Fig. 6C-F). The most obvious NHR-23-depletion phenotype was an increase in the meiotic division zone (Div); large numbers of detached spermatocytes containing metaphase-like chromosomes with associated microtubule spindles (Fig. 6D). Recently detached spermatocytes had relatively normal diakinesis and metaphase I spindles, but metaphase chromosome alignment was impaired. Slightly older spermatocytes had more dispersed chromosomes (M*) and multipolar asters with four or more asters (Fig. 6F). In control germlines, anti-pHisH3(ser10) labelled chromosomes through both meiotic divisions and only became undetectable in post-meiotic budding figures (Fig. 6E). In NHR-23-depleted germlines, pHisH3 labelling persisted in arrested, metaphase-like cells (M*, Fig. 6F). The very oldest spermatocytes exhibited a distinct terminal/late arrest phenotype; these spermatocytes lacked microtubule spindles and their chromosomes had aggregated into one or more tight masses and failed to label with anti-pHis3(ser10) (Fig. 6F). To assess CDK-cyclin B activity, gonads were labelled for a phospho-epitope primarily found in proteins phosphorylated at inception of mitosis or meiosis (MPM2). In control spermatocytes (Fig. 6G), MPM2 labelling turned on during late meiotic prophase (karyosome stage), remained high through meiotic divisions, and then dropped abruptly during post-meiotic partitioning. In NHR-23-depleted spermatocytes (Fig. 6H), MPM2 labelling remained high in metaphase-arrested spermatocytes, only dropping in terminal arrest spermatocytes. Anti-nuclear pore antibodies confirmed that nuclear envelope breakdown occurred in a timely fashion in both control and NHR-23-depleted spermatocytes (Fig. 6I,J). Together, these results suggest that the cell cycle regulators of M-phase entry are unaffected by NHR-23-depletion. However depleted spermatocytes remain in a prolonged prometaphase state, develop multipolar spindles and never progress to anaphase. M-phase markers do eventually turn-off, but only in late, terminal stage spermatocytes.

We hypothesized that the observed meiotic defects might arise from earlier defects during the poorly understood karyosome stage (Fig. 1)(Shakes et al., 2009). In control gonads labelled with an antibody against active RNA polymerase II, entry into the karyosome stage was marked by abrupt cessation of global transcription (Fig 6K) (Shakes et al., 2009). In NHR-23-depleted gonads, turn-off of global transcription was both delayed and more gradual (Fig 6L). In a complementary fashion, the turn-on of pHisH3(ser10) labelling, which corresponds to chromosome condensation, was also delayed and more gradual (Fig. 6D,F). Closer examination revealed that, during the karyosome stage, the chromosomes in both control and depleted spermatocytes properly detached from the nuclear envelope, but the compaction of chromosomes into a single tight mass was more limited in NHR-23-depleted spermatocytes (Fig. 6I,J, karyosome nuclei labeled "K"). Such aberrations in chromosome compaction during karyosome stage might contribute to subsequent defects in meiotic chromosome segregation as well as the prolonged M-phase arrest, if such defects trigger a cell cycle checkpoint.

NHR-23-depleted spermatocytes have defects in both cytokinesis and post-meiotic partitioning

In previous studies, a metaphase I arrest of the cell cycle was not sufficient to block other aspects of sperm development. Notably, spermatocytes lacking a functional anaphase promoting complex arrest in metaphase I but still undergo post-meiotic partitioning to generate motile, albeit anucleate, sperm (Golden et al., 2000; Sadler and Shakes, 2000). Although NHR-23-depleted germlines do not make mature spermatids, we wondered if they nevertheless attempted aspects of normal, post-meiotic partitioning and residual body formation which is mediated in part by actin microfilaments (Hu et al., 2019; Winter et al., 2017). In control spermatocytes, actin localization to the cortex was uniform in metaphase and enriched in cortical rings during anaphase (Fig. 6K). In partitioning stage spermatocytes, actin localized in a central band and ultimately degraded with the residual body (RB; Fig. 6M). In NHR-23-depleted spermatocytes, actin patterns remained largely cortical in both metaphase arrested and late terminally arrested spermatocytes (Fig. 6N). Consistent with our DIC

analysis, NHR-23-depleted spermatocytes showed no evidence of cytokinesis or residual body formation.

NHR-23 is required for biogenesis of sperm-specific fibrous body-membranous organelle (FB-MO) complexes.

Among *C. elegans* mutants with spermatogenesis defects, several exhibit a spermatocyte-arrest phenotype. Four of these (*spe-4*, *spe-5*, *spe-6*, and *wee-1.3*) exhibit a vacuolated phenotype by DIC that is very similar to NHR-23-depleted spermatocytes (Fig. 7A). Other spermatocyte arrest mutants (*spe-39*, *spe-44*) do not exhibit the same vacuolated phenotype (Fig. 7A)(Kulkarni et al., 2012; Zhu and L'Hernault, 2003). In previous studies, transmission electron microscopy found these vacuoles are swollen, distended membranous organelles (MOs) (Lamitina and L'Hernault, 2002; L'Hernault and Arduengo, 1992; Machaca and L'Hernault, 1997; Varkey et al., 1993). To determine if vacuoles in NHR-23-depleted spermatocytes were MOs, we crossed a PEEL-1::GFP transgene into our *mex-5p*::*TIR1*, *nhr-23::GFP::AID*::3xFLAG* strain. PEEL-1 is the toxin component of a toxin-antidote selfish genetic element (Seidel et al., 2008) that also serves as a useful MO marker (Seidel et al., 2011). In control primary spermatocytes and budding figures, PEEL-1::GFP marked internal membranes (Figs 1 and 7B). In mature spermatids, PEEL-1::GFP exhibited a bright punctate pattern corresponding to plasma membrane-docked MOs. In NHR-23-depleted spermatocytes, PEEL-1::GFP colocalized with vacuoles in the corresponding DIC images (Fig. 7B), indicating that MOs form but then vacuolate in terminal arrest spermatocytes.

In developing spermatocytes, MOs serve as sites where Major Sperm Protein (MSP) assembles into fibrous bodies (FBs) (Fig. 7C). MSP is a nematode-specific protein which drives the actin-like cell motility of spermatozoa while also serving as a signaling molecule for oocyte maturation (Miller et al., 2001). Not surprisingly, MO defects are often associated with either abnormalities in FB assembly as in *spe-5* and *spe-39* mutants (Machaca and L'Hernault, 1997; Zhu and L'Hernault, 2003) or a complete failure in FB formation as in *spe-6* and *spe-44* (Kulkarni et al., 2012; Varkey et al., 1993). In wildtype animals, MSP is first expressed in mid-pachytene spermatocytes and, by the end of the karyosome stage, individual spermatocytes fill with discrete, uniformly sized FBs (Fig. 7D)(Chu and Shakes, 2013). During post-

meiotic partitioning, FB-MO complexes facilitate MSP delivery to spermatids. In NHR-23-depleted spermatocytes, MSP was expressed, but in most spermatocytes, it remained dispersed throughout the cytoplasm (Fig. 7D). NHR-23-depleted germlines sometimes included individual spermatocytes with MSP assemblages (Fig. 7D, asterisk) that were more variable in shape and size than normal FBs.

To investigate potential defects in FB-MO biogenesis, gonads were immunolabelled with 1CB4, an antibody labelling glycosylated MO proteins (Okamoto and Thomson, 1985). In control gonads, 1CB4 labelled discrete cytoplasmic organelles starting in mid-pachytene spermatocytes (Fig. 7E inset). This pattern persisted until the spermatid stage when individual MOs docked with the plasma membrane (Fig. 1D, 7E). In NHR-23-depleted germlines, the 1CB4 pattern in pachytene spermatocytes was similar to controls (Fig. 7E inset). However, in arrested 1° spermatocytes, MOs aggregated into clumps adjacent to the plasma membrane, suggesting a defect in either MO docking or later stages of MO morphogenesis.

Of the spermatocyte arrest mutants shown in Fig. 7A, only the *spe-44* gene encodes an early transcriptional regulator (Kulkarni et al., 2012). Like NHR-23-depleted spermatocytes, *spe-44* spermatocytes exhibit defects in MSP assembly and meiotic progression (Kulkarni et al, 2012). However, *spe-44* spermatocytes arrest in the second rather than the first meiotic division, and arrested spermatocytes do not fill with distended MOs (Fig. 7A). We confirmed that SPE-44 depletion causes sterility, as previously reported (Fig. S4A)(Kasimatis et al., 2018). To determine whether NHR-23 and SPE-44 play similar or distinct roles in spermatogenesis, we compared 1CB4 patterns as a proxy for their role in FB-MO biogenesis. In SPE-44-depleted pachytene spermatocytes, the 1CB4 pattern within developing spermatocytes did not form discrete structures (Fig. 7E inset), matching the published pattern for *spe-44(ok1400)* mutants (Kulkarni et al., 2012). As this *spe-44* pattern is distinct from NHR-23-depletion defects, we also examined doubly depleted males which typically exhibited a more severe synthetic phenotype (Fig. 7E).

NHR-23 and SPE-44 independently regulate spermatogenesis

The synthetic FB-MO phenotype observed following NHR-23+SPE-44 double depletion raised the possibility that these regulators could function in distinct

pathways. In *spe-44*(*ok1400*) mutants, levels of *nhr-23* mRNA do not differ significantly from wildtype (Kulkarni et al., 2012). To test whether SPE-44 might function downstream of NHR-23, we generated a strain carrying an *mScarlet::3xMyc* cassette inserted into the 3' end of *spe-44* by CRISPR/Cas9-mediated genome editing. There is only a single *spe-44* isoform and our strain results in a C-terminal translational fusion. We confirmed that the tag did not compromise SPE-44 function, as animals with the *mScarlet::3xMyc* knock-in had a wildtype brood-size (Fig. S4B), and SPE-44::mScarlet::3xMyc localization was similar to previous reports (Fig. 8A) (Kulkarni et al., 2012). On control media, spermatocytes in strains carrying both *spe-44::mScarlet::3xMyc* and *mex-5*::*TIR1*, *nhr-23::GFP::AID*::3xFLAG* exhibited an almost complete overlap in expression for SPE-44 and NHR-23 (Fig. 8A). When grown on auxin, depletion of NHR-23 did not affect the level or expression pattern of SPE-44::mScarlet::3xMyc. These data indicate NHR-23 regulates neither SPE-44 expression nor its localization.

These data raised the possibility that *C. elegans* spermatogenesis is coordinated by multiple transcriptional regulatory pathways. If so, then spermatogenesis-specific genes like *spe-11* that are known not to be regulated by SPE-44 may instead be NHR-23 target genes. We acquired a strain in which the *spe-11* promoter drives expression of an *mCherry::*Histone *H2B::unc-54 3'UTR* reporter (Frøkjaer-Jensen et al., 2008). We crossed AID* alleles of *nhr*-23 (Zhang et al., 2015) and *spe-44* (Kasimatis et al., 2018) lacking a fluorescent protein fusion, as well as a *mex-5p::TIR1* allele, into this *spe-11* reporter strain. In animals grown on control media, the *spe-11* promoter drove mCherry-histone expression starting in pachytene spermatocytes with the histone fusion protein persisting in spermatids (Fig. 8B)(Frøkjaer-Jensen et al., 2008). Following individual depletion of either NHR-23 or SPE-44, expressed mCherry fusion protein persisted in meiotically arrested nuclei despite the spermatocyte defects and their meiotic arrest in meiosis I or II, respectively. To test whether NHR-23 and SPE-44 redundantly regulated *spe-11*, we created a *spe-11* reporter strain that would allow simultaneous germline-specific depletion of NHR-23 and SPE-44. Co-depletion of NHR-23 and SPE-44 resulted in germline defects so severe that it was difficult to identify individual cells within the proximal gonad. Yet, reporter expression was still detectable in nuclei (Fig. 8B). Together these results suggest not only that NHR-23 and SPE-44 function in independent pathways, but also that *spe-11* is regulated either

by factors upstream of NHR-23 and SPE-44 or by an additional, yet to be identified transcriptional regulatory pathway (Fig. 8C).

Discussion

C. elegans spermatogenesis offers a powerful model to define how gene-regulatory networks implement and coordinate the cell cycle and developmental programs. In this study, we identify NHR-23 as a critical regulator of spermatogenesis in both hermaphrodite and male animals.

NHR-23 is expressed in 1º spermatocytes and acts in the L4 stage in hermaphrodites. NHR-23 functions downstream of the sex determination pathway (Fig. 4), and inactivation in hermaphrodite germlines causes a loss of mature spermatids (Fig. 3-5). However, cells recognizable as 1º spermatocytes developed (Fig. 5-7) and progressed through meiotic prophase (Fig. 6). Numerous cell cycle markers indicated that affected spermatocytes entered but did not complete meiosis. Instead, the fully condensed chromosomes clustered within a disorganized and ultimately multipolar microtubule array (Fig. 6). Although microtubules appeared to associate with the chromatin, there was no evidence of even attempted anaphase segregation (Fig. 6). Similarly, we never observed cytokinesis or spermatid budding divisions. The oldest cells contained terminal chromatin masses, which may represent either a variation of normal sperm chromatin remodeling or apoptotic compaction (Fig. 6). In addition to these meiotic roles, NHR-23 is necessary for proper FB-MO biogenesis. Golgi-derived MOs developed in meiotic prophase spermatocytes, yet MSP failed to assemble into associated FBs and the morphology of MOs in arrested spermatocytes was clearly abnormal (Fig. 7).

Multiple gene regulatory networks may control *C. elegans* spermatogenesis

The meiotic phenotypes following NHR-23-depletion are similar to but distinct from those caused by inactivation of *spe-44*, a critical transcriptional regulator of spermatogenesis (Fig. 8C). In both NHR-23-depletion and *spe-44* mutants, meiotic prophase is largely unaffected except that chromatin compaction is delayed during the karyosome stage (Kulkarni et al., 2012). *spe-44* spermatocytes also fail to assemble MSP into FBs (Kulkarni et al., 2012). Both NHR-23 and SPE-44 proteins are first

expressed in developing spermatocytes and have similar mRNA expression profiles in a spatiotemporal analysis of germline expression (Tzur et al., 2018). NHR-23 and SPE-44 both function downstream of the canonical sex determination pathway (Fig. 4) (Kulkarni et al., 2012). While both are essential to complete the spermatocyte meiotic divisions, NHR-23 is necessary for the first meiotic division (Fig. 6), whereas SPE-44 is necessary for the second meiotic division (Fig. 8C)(Kulkarni et al., 2012). Their microtubule spindle patterns also differ; in NHR-23-depleted spermatocytes the microtubule asters remain close to the chromosomes and cell center (Fig. 6D,F), whereas those in *spe-44* mutants move to the cell cortex (Kulkarni et al., 2012) SPE-44 regulates ELT-1 (del Castillo-Olivares et al., 2009; Kulkarni et al., 2012), which promotes MSP gene expression in conjunction with a histone methyltransferase, SET-17 (Engert et al., 2018). However, SPE-44 does not regulate *nhr-23* (Kulkarni et al., 2012), nor does NHR-23-depletion affect SPE-44 expression (Fig. 8A) consistent with these two transcription factors regulating distinct pathways. Co-depletion of NHR-23 and SPE-44 led to additive phenotypes such as reduction of the MO marker 1Cb4 (Fig. 7E) and more severe germline morphology defects (Fig. 8B). NHR-23-depleted spermatocytes developed distended MOs similar to those of several sperm function mutants (e.g. *spe-4(lf), spe-6(lf), wee-1.3(gf)*)(Lamitina and L'Hernault, 2002; L'Hernault et al., 1988; Muhlrad and Ward, 2002; Varkey et al., 1993). *spe-44* does not regulate these genes (Kulkarni et al., 2012) and does not exhibit this mutant phenotype (Kulkarni et al., 2012) (Fig. 7A). These results suggest that NHR-23 and SPE-44 function in separate pathways to regulate distinct cellular processes.

Additional undiscovered gene regulatory pathways are likely to help execute the *C. elegans* spermatogenesis program. *spe-11p::mCherry::H2B* reporter activity was unaffected by NHR-23, SPE-44, or NHR-23+SPE-44 depletions. These data could suggest the presence of three or more distinct pathways controlling sperm morphogenesis in *C. elegans*, or alternatively *spe-11* is directly regulated by a factor upstream of both NHR-23 and SPE-44 (Fig. 8C). Notably, SPE-44 only accounts for one-quarter of sperm-expressed genes (Kulkarni et al., 2012). As we further characterize NHR-23 and SPE-44, it will be informative to compare their function to spermatogenesis regulators in other systems. In *Drosophila,* BAM promotes differentiation of spermatogonia into spermatocytes (McKearin and Spradling, 1990), while the sperm-specific transcriptional program is promoted by two complexes:

tMAC and tTAF (Beall et al., 2007; Laktionov et al., 2018; Metcalf and Wassarman, 2007). In mice, retinoic acid receptor signaling promotes both spermatogonia differentiation and meiotic entry (Chung et al., 2004; Gely-Pernot et al., 2012; Gely-Pernot et al., 2015), and MYBL1 coordinates the expression of four downstream transcription factors (CREM-τ, TRF2, RFX2 and Sox30) (Bolcun-Filas et al., 2011; Horvath et al., 2009; Li et al., 2013; Zhang et al., 2018). Zhang *et al.* (2018) suggest that tree-like regulatory cascades would be more efficient than a network enriched in nodes. Spermatogenesis is a rapidly evolving process. Defining the regulatory architecture across a range of model organisms will shed insight into conserved features controlling sperm morphogenesis as well as distinctive features which have evolved separately in mammals, insects, nematodes, and other organisms (White-Cooper and Bausek, 2010).

Circadian rhythm regulators in spermatogenic tissues

Previous to this study, the best characterized role for *nhr-23* in *C. elegans* was as a key regulator of molting (Frand et al., 2005; Kostrouchova et al., 1998; Kostrouchova et al., 2001; Kouns et al., 2011; Patel and Frand, 2018). Like many molting factors, *nhr-23* mRNA levels oscillate over the course of each larval stage (Gissendanner et al., 2004; Hendriks et al., 2014; Kostrouchova et al., 2001). Yet in sperm-producing germlines, NHR-23 is expressed constitutively, suggesting a radically different mode of regulation in soma vs. germ tissues. Interestingly, many core mammalian circadian rhythm regulators also oscillate in the soma but exhibit constitutive, non-oscillatory expression in the testes (Alvarez et al., 2008; Kang et al., 2010; Kennaway et al., 2012; Morse et al., 2003). Although the non-circadian roles of these factors in spermatogenesis have not been deeply explored, null male mice of the clock gene BMAL1 have fertility defects and are difficult to mate (Alvarez et al., 2008), and depletion of the NHR-23 homolog, RORα/NR1F1, in rat Sertoli cells reduces sperm count (Mandal et al., 2018). It remains unclear how these timers have been co-opted to promote spermatogenesis. Our work may provide an entry point into understanding both the function of these circadian rhythm factors during spermatogenesis and how their expression is altered from oscillating to constitutive expression in the testes.

Future perspectives

Most known spermatogenesis regulators have been identified in forward genetic screens and candidate-based testing of male germline-enriched factors. These approaches have been incredibly powerful but would miss factors such as NHR-23 which also have earlier essential roles in embryogenesis and molting. Similarly, as NHR-23 is maternally loaded, it was not identified by focusing on male enriched transcriptional regulators (Ebbing et al., 2018; Kulkarni et al., 2012; Reinke et al., 2004; Tzur et al., 2018). High-throughput GFP::AID* tagging of NHR-23-regulated genes could provide an exciting avenue for identifying novel regulators of spermatogenesis. New datasets that detail mRNA expression with respect to position in the germline can also be analyzed to identify transcriptional regulators expressed before, coincident with, and after the NHR-23/SPE-44 zone of expression. The mammalian homologs of NHR-23 are regulated by several sterol ligands (Kallen et al., 2002; Kallen et al., 2004; Soroosh et al., 2014; Wang et al., 2010), raising the exciting possibility that hormonal signaling through NHR-23 coordinates spermatogenic and somatic development events. Going forward, determining factors that either regulate or are regulated by NHR-23 and SPE-44 will deepen our understanding of how the NHR-23 node controls spermatogenesis and how gene regulatory networks control the complex cellular events underpinning sperm morphogenesis.

Materials and Methods

Strains and Culture

C. elegans were cultured as originally (Brenner, 1974), except worms were grown on MYOB media instead of NGM. MYOB agar was made as previously described (Church et al., 1995).

Strains used in this study:

N2 (Bristol)

JDW5 *nhr-23(wrd1[GFP^BioTag::AID*::3xFLAG])* I*; ieSi38 [Psun-1::TIR1::mRuby::sun-1 3'UTR, cb-unc-119(+)]* IV

JDW26 *nhr-23(wrd1[GFP^BioTag::AID*::3xFLAG])* I/*hT2[bli-4(e937) let-?(q782) qIs48]* (I;III) ; *ieSi38 [Psun-1::TIR1::mRuby::sun-1 3'UTR, cb-unc-119(+)]* IV

JDW29 *nhr-23(wrd8[nhr-23::GFP^degron::3xFLAG])* I

JDW32 *fog-3(wrd6[fog-3 N-term STOP with frameshift]), nhr-23(wrd1[GFP^BioTag::AID*::3xFLAG])* I*/hT2[bli-4(e937) let-?(q782) qIs48]* (I;III)*; ieSi38 [Psun-1::TIR1::mRuby::sun-1 3'UTR, cb-unc-119(+)]* IV

JDW40 *wrdSi11(mex-5p::TIR1:F2A:mTagBFP2:tbb-2 3'UTR), nhr-23(wrd8[nhr-23::GFP^AID*::3xFLAG])* I

JDW45 *wrdSi12(mex-5p::TIR1:F2A:mTagBFP2:tbb-2 3'UTR), nhr-23(wrd8[nhr-23::GFP^AID*::3xFLAG])* I*; fem-3(q20)* IV

JDW47 *wrdSi13(mex-5p::TIR1:F2A:mTagBFP2:tbb-2 3'UTR), nhr-23(wrd8[nhr-23::GFP^AID*::3xFLAG])* I*; fbf-1(ok91), fbf-2(q704)/mIn1 [dpy-10(e128) mIs14]* II

JDW86 *wrdSi15(mex-5p::TIR1:F2A:mTagBFP2:tbb-2 3'UTR)* I*; spe-44(fx110[spe-44::AID*])* IV*; him-5(e1490)* V

JDW87 *wrdSi16(mex-5p::TIR1:F2A:mTagBFP2:tbb-2 3'UTR), nhr-23(wrd8[nhr-23::GFP^AID*::3xFLAG])* I*; him-5(e1490)* V

JDW89 *wrdSi18(mex-5p::TIR1:F2A:mTagBFP2:tbb-2 3'UTR)* I

JDW92 *wrdSi19(mex-5p::TIR1:F2A:mTagBFP2:tbb-2 3'UTR), nhr-23(kry61[nhr-23::AID*::TEV::3xFLAG])* I; *him-5(e1490)* V

JDW101 *spe-44(wrd20[spe-44::30 amino acid linker::mScarlet^3xMyc])*

JDW146 *wrdSi19(mex-5p::TIR1:F2A:mTagBFP2:tbb-2 3'UTR), nhr-23(kry61[nhr-23::AID*::TEV::3xFLAG*]) I; *spe-44(fx110[spe-44::AID*])* IV; *him-5(e1490)* V

KRY87 *nhr-23(kry61(nhr-23::AID*::TEV::3xFLAG))I* (Zhang et al., 2015)

The following strains were provided by the *Caenorhabditis Genetics Center*:

BA676 *spe-6(hc92) unc-32(e189)* III; *eDp6* (III;f)

BA714 *sDf5/spe-4(hc78)* I

BA763 *spe-5(hc93)* I; *sDp2* (I;f)

DR466 *him-5(e1490)* V

DS179 *spe-8(hc50) I; him-8 (e1489) IV*

PX627 *fxIs1 I; spe-44(fx110[spe-44::degron]) IV* (Kasimatis et al., 2018)

SL753 *spe-39(tx12) V/nT1 [unc-?(n754) let-?]* (IV;V)

SL940 *wee-1.3(q89eb94) unc-4(e120)/mIn1 [dpy-10(e128) mIs14]* II

The following was a gift from Erik Jorgensen and is currently unpublished:
EG9615 *oxSi1091 [Pmex-5::Cas9(smu-2 introns) unc-119+]* II; *unc-119(ed3)* III

Immunocytochemistry

Intact gonads were obtained by dissection of individual males in 5-10 microliters of egg buffer (Edgar, 1995) on ColorFrost Plus slides (Fisher Scientific #12-550) coated with poly-L-lysine (Sigma Aldrich #P8290). Samples were freeze-cracked in liquid nitrogen. Sperm spreads to analyze detached spermatocytes and spermatids were obtained by applying slight pressure to the coverslip before freeze-cracking. Most samples were fixed overnight in -20°C methanol. Specimen preparation and antibody labeling followed established protocols (Shakes et al., 2009). Primary antibodies included: 1:100 Alexa Fluor 488-conjugated anti-α-tubulin (mouse monoclonal DM1A, Millipore-Sigma #16-323), 1:200 rabbit anti-phosphorylated histone H3 (S10) (Millipore #06-570, Lot 2649123), 1:100 MPM-2 mouse monoclonal (EMD Millipore #05-368), 1:200 anti-nuclear pore antibody Mab414 (Abcam ab24609), 1:250 anti-RNA polymerase II CTD repeat Ser2 (Abcam #ab5095), 1:200 rabbit anti-SPE-44 (Kulkarni et al., 2012), 1:15,000 G3197 rabbit anti-MSP polyclonal (Kosinski, 2005; gift from David Greenstein, University of Minnesota), and 1:40 1CB4 monoclonal (Okamoto and Thomson, 1985; gift from Steve L'Hernault, Emory University). All samples were incubated with primary antibodies for 2 hours at room temperature except MPM-2 samples which were incubated overnight at 4°C. Affinity-purified secondary antibodies included 1:300 Alexa Fluor Plus 555 goat anti-rabbit IgG (Invitrogen #A32732) and 1:100 Alexa Fluor 488 Goat anti-mouse IgG (H+L) (Jackson ImmunoResearch #115-545-146).

Final slides were mounted with DAPI containing Fluoro Gel II mounting medium (Electron Microscopy Sciences #50-246-93). Images were acquired under differential interference contrast or epifluorescence using an Olympus BX60 microscope equipped with a QImaging EXi Aqua CCD camera. Photos were taken, merged, and exported for analysis using the program iVision. In some cases, the levels adjust function in Adobe Photoshop was used to spread the data containing regions of the image across the full range of tonalities. When the experiment was designed to compare levels of fluorescence between control and experimental samples, images from the same experimental preparation were captured with the same exposure and any post-experimental processing

were done identically. However, when the critical imaging information was to distinguish between the structures of chromatin, microtubule array, or 1CB4 staining structures, the images were optimized for the individual cells.

For actin staining, slides with dissected gonads were fixed for 10 min in 4% fresh paraformaldehyde (FisherScientific) in 1x PBS. Samples were quenched in 1 M glycine (FisherScientific) in PBS (FisherScientific #BP3994) for at least 5 min, permeabilized in 0.1% Triton-X-100 (FisherScientific #BP151) in PBS for 5 min, then dip washed in 1xPBS. Slides were incubated with rhodamine-conjugated phalloidin (Invitrogen #R415) diluted 1:100 in 1xPBS for 15 min in the dark before washing three times in PBS for 5 min each. Slides were mounted as above.

For DIC/Hoechst preparations, males were dissected in egg buffer with 100 mg/ml Hoechst 33342 (Sigma Aldrich #94403) on non-plus slides and immediately imaged as according to Edgar, 1995.

CRISPR/Cas9 Genome Editing

A thorough description of the plasmids and oligonucleotides described in this section is provided in Table S1 and S2, respectively.

nhr-23(wrd1[GFP^BioTag::AID::3xFLAG])* was generated using a pJW1598 repair template, based on the previously described set of self-excising cassette (SEC) vectors for genome editing . Briefly, *nhr-23* 5' and 3' homology arms were PCR amplified from N2 genomic DNA and Gibson cloned into a AvrII+SpeI double-digested pJW1592 vector (Ashley et al., 2020) as described in (Dickinson et al., 2015). N2 animals were injected and knock-ins were recovered as previously described (Dickinson et al., 2015)A previously described Cas9+sgRNA plasmid (pJW1254) (Zhang et al., 2015)targeting the 3' end of *nhr-23* was used to generate the knock-in.

nhr-23(wrd8[nhr-23::GFP^AID::3xFLAG])* was generated with the self-excising cassette (SEC method (Dickinson et al., 2015) using a pJW1725 (nhr-23:GFP:SEC:degron:3XFLAG with *nhr-23* homology arms, U6p::sgRNA) repair template. The repair template (pJW1725) was constructed using SapTrap (Schwartz and Jorgensen, 2016) cloning with an SEC selection block (Dickinson et al., 2018). The

5’ homology arm was PCR amplified from a gBlock (IDT) and contained silent mutations to inactivate the PAM and two SapI restriction sites. The 3’ homology arm was PCR amplified from N2 genomic DNA. The 5’ and 3’ homology arm PCRs were cloned into pCR-Blunt II-TOPO using a Zero Blunt™ TOPO™ PCR Cloning Kit (Invitrogen, catalog #450245) to generate pJW1776 and pJW1781, respectively. pJW1725 was assembled through SapTrap cloning using pDD379 (backbone), pMLS287 (flexible linker), pDD372 (GFP), pDD363 (SEC), pJW1659 (linker::AID*::3xFLAG, pJW1776 (5’ homology arm), pJW1781 (3’ homology arm), and annealed oligos 3488+3489 (*nhr-23* targeting sgRNA) (Tables S1 and S2). The plasmid was injected into EG9615, which stably expresses Cas9, and knock-in animals were recovered as described (Dickinson et al., 2015). The strain was outcrossed two times to remove the *mex*-5p::*Cas9* allele and the SEC was excised to make JDW29.

spe-44(wrd20[spe-44::30 amino acid linker::mScarlet^3xMyc]) was generated using SapTrap cloning with an SEC cassette, similar to the approach described above. Oligos 3916+3917 were annealed and Sap Trap cloned (Schwartz and Jorgensen, 2016) into pJW1838 {Ashley:2020ib}to generate pJW1872(*U6p::sgRNA (F+E)* targeting *spe-44*). A pJW1876 repair template (30 amino acid flexible linker::mScarlet^SEC (Lox511I)^3xMyc with *spe-44* homology arms) was previously described (Ashley et al., 2020). The plasmid was injected into EG9615 and knock-in animals were recovered as described (Dickinson et al., 2015). The strain was outcrossed 2 times to remove the *mex*-5p::*Cas9* allele and the SEC was excised to make JDW101.

wrdSi10 was generated with the self-excising cassette method (Dickinson et al., 2015) and a recently described TIR::F2A::mTagBFP2 construct (Ashley et al., 2020). pJW1357 (*mex-5*p::*TIR1:F2A:mTagBFP2*) (Ashley et al., 2020) and pCZGY2747 (*eft-3p::Cas9;* LGI ttTi4348 sgRNA vector) injected into JDW29 to make JDW39. *wrd10* was subsequently outcrossed to N2 animals one time to generate JDW84, then heat-shocked at 34°C for 2-3 hours to excise the SEC to make JDW89. These two strains carrying a *mex-5*p::*TIR1:F2A:mTagBFP2* with and without the SEC, respectively are part of our recent AID toolkit and sre available through the *Caenorhabditis* Genetics Center.

wrdSi12, 13 and 16 were made by crossing JDW39 to JK816 [*fem-3(q20) IV*], JK3107 [*fbf-1(ok91) fbf-2(q704)*/mIn1 [*dpy-10(e128) mIs14*] II], and DR466 [*him-5(e1490) V*], respectively. *wrdSi19* was made by crossing KRY87 [*nhr-23[kry61(nhr-23::AID*-TEV-3xFLAG)*]] I to JDW83 [wrdSi10(*mex-5p::TIR1:F2A:mTagBFP2:tbb-2 3'UTR+SEC, I:-5.32*); *him-5(e1490) V*]. The Rol phenotype produced by expression of the dominant *sqt-1* allele within the SEC was used as a genetic marker to follow the insertion. Once the resultant strains were established, the SEC was excised by heat shock for 2-3 hours at 34°C in those strains, thereby making JDW45, JDW47, JDW87 and JDW92, respectively.

Plasmid sequences are available upon request.

JDW32 *[fog-3(wrd6)]* was made by ribonucleoprotein-based co-CRISPR injection into JDW29 (Arribere et al., 2014; Paix et al., 2015). sgRNAs were generated by *in vitro* transcription of PCR templates, as described by (Leonetti et al., 2016). JDW29 animals were injected with 3.8 µM *dpy-10* sgRNA, 25.0 µM *fog-3* sgRNA, 15.1 µM Cas9 protein, 0.4 µM *dpy-10* repair oligo, 1.5 µM *fog-3* repair oligo. The sequence of the sgRNAs and repair oligos is provided in Table S3. The insertion was targeted to the middle of exon 2 in the *fog*-3 locus and contained an *Eco*RI site to facilitate genotyping, followed by an in-frame stop codon. An additional base was inserted after the stop codon to produce a frameshift. F1 rollers were selected and screened by PCR and restriction digestion as described previously (Ward, 2015).

Western Blot

Gravid JDW87 adults were allowed to lay eggs for 1 hour on MYOB with and without 4 mM auxin (Indole 3-acetic acid, Alfa Aesar #AAA1055622), then removed. Progeny were allowed to grow until L4 + 1 day at 20°C. 100 hand-picked males were collected, washed 3X in M9 with 0.05% gelatin (VWR #97062-620) and resuspended in 30 µl M9+gelatin. Worms were freeze/thawed 3X in liquid nitrogen and 10 µl Laemmli sample buffer with 10% BME was mixed in. Samples were boiled for 10 minutes at 95°C, centrifuged for 5 minutes at full speed and the supernatant was removed to a new tube. Proteins were separated on a SDS-PAGE Mini-PROTEAN TGX 4-15% gradient gel (Bio-Rad, catalog #456-1086) along a 1:1 mix of Amersham ECL Rainbow Molecular Weight Markers (Amersham # 95040-114) and Precision Plus Protein™

Unstained Standards #1610363. Proteins were transferred to a PVDF membrane using a Trans-Blot Turbo Transfer System. Membrane was washed in TBST and blocked in TBST + 5% milk (VWR # 10128-600) for 1 hour at room temperature. Membrane was incubated in TBST + 1:1000 Anti-FLAG-M2-HRP (Sigma, #8592) at 4°C overnight while rolling, washed 5X in TBST and incubated in 10ml Supersignal West Femto Maximum Sensitivity Substrate (Thermo Scientific Pierce #34095) for 5 minutes. Separated proteins on the gel, transferred proteins on the PVDF and the final blot were imaged using the "chemi high-resolution" setting on a Bio-Rad ChemiDoc MP System. For depletion quantitation, the blot images were taken to avoid pixel saturation, and the number of pixels in each band were quantified using a densitometry feature in ImageLab software (Bio-Rad). Percent depletion was calculated by: [(pixels in control band-pixels in depletion band)/(pixels in depletion band)]x100%.

Auxin Depletion

Control media consisted of MYOB agar + 0.25% ethanol. Auxin media was made by dissolving indole 3-acetic acid in 100% ethanol to 1.6M and then mixing it into melted MYOB agar at 55°C to a final concentration of 4 mM prior to pouring plates. Temperature of the media was monitored with a Lasergrip 1080 infrared thermometer gun (Etekcity). For live progeny counts, gravid adults were allowed to lay F1 eggs for 1 hour on control or auxin media and then removed. F1 progeny grew at 20°C until L4, then were individually placed onto equivalent media and allowed to lay eggs for 24 hours (n=12 per condition). These worms were transferred to a new and equivalent set of media each day for 3 days and F2 eggs were counted. Once the F2 progeny of these worms grew to L4, they were counted. For matings, F1 hermaphrodite progeny were grown to L4, then individually picked to plates and either left alone or mated with males (picked as L4s) for 24 hours at 20°C. Transfers and counts were then performed as described. To determine the auxin-sensitive period of development, F1 progeny eggs were laid on MYOB media + ethanol with or without 4 mM auxin, allowed to grow until the appropriate stage and were transferred to the opposite plate-type for the duration of their development. Once F1 progeny reached L4 + 1 day, transfers began as described and F2 progeny were counted. For cell morphology and immunohistochemistry, worms were grown from the late L1 stage on 4 mM auxin media.

Co-suppression

nhr-23 cDNA was PCR amplified and Gateway cloned (Invitrogen) into pDONR221 to produce pJW258. The *mex-5* promoter was amplified from *C. elegans* N2 genomic DNA and an *nhr-23* cDNA was amplified from pJW258. PCR stitching was used to create a chimeric *mex-5p::nhr-23* cDNA PCR product, as previously described (Dernburg et al., 2000). 50 ng/µl was injected into JDW45 *[fem-3(q20)]* hermaphrodites along with 10 ng/µl pCFJ90 *[Pmyo-2::mCherry::unc-54utr]*, a pharyngeal-expressed co-injection marker. Worms were incubated at 25°C to masculinize the germlines of the subsequent F1 progeny. *myo-2p::mCherry* positive F1 young adults were then imaged for defective/arrested spermatocytes.

Mating/Transactivation

In a variant of a transactivation experiment (Shakes and Ward, 1989), single *spe-8* L4 hermaphrodites were crossed to three NHR-23-depleted or control males at room temperature (22°C). Controls included unmated *spe-8* hermaphrodites as well as crossing to *him-5* males or males containing the NHR-23 auxin construct that were grown on non-auxin plates. After 24 hours, the males were removed. The mated *spe-8* hermaphrodites were transferred to fresh plates daily, and the size of each brood was counted. For the crosses involving NHR-23-depleted males, L4 hermaphrodite progeny were assessed for self-fertility as an indicator of genotype (infertile SPE self-progeny resulting from transactivation or fertile spe/+ outcross progeny). For the crosses involving NHR-23-depleted males, one set of crosses was performed with young adult males (L4 + 24 hrs) to potentially deplete the males of their earliest produced sperm.

Statistical analyses

Statistical tests and numbers of animals analyzed are detailed in figure legends.

Acknowledgements

We thank Diana Chu and Penny Sadler for their critical reading of this manuscript.

Competing Interests

No competing interests declared.

Funding

This work was funded by the National Institute of Health (NIH) National Institute of General Medical Sciences (NIGMS) [R00GM107345 to JDW and R15GM096309 to DCS] and the National Science Foundation (NSF) Division of Molecular and Cellular Biosciences (CAREER award 1942922). Some strains were provided by the *Caenorhabditis* Genetics Center, which is funded by the NIH Office of Research Infrastructure Programs [P40 OD010440].

Author Contributions

J.M.R., R.M.M., D.C.S., and J.D.W. designed the experiments. All authors performed the experiments. J.M.R., A.L.A, D.C.S., and J.D.W. performed the data analyses. J.M.R., K.N.M., D.C.S., and J.D.W. wrote the paper with feedback from the other authors.

References

Akashi, M. and Takumi, T. (2005). The orphan nuclear receptor RORalpha regulates circadian transcription of the mammalian core-clock Bmal1. *Nature Structural & Molecular Biology* **12**, 441–448.

Alvarez, J. D., Hansen, A., Ord, T., Bebas, P., Chappell, P. E., Giebultowicz, J. M., Williams, C., Moss, S. and Sehgal, A. (2008). The circadian clock protein BMAL1 is necessary for fertility and proper testosterone production in mice. *J. Biol. Rhythms* **23**, 26–36.

André, E., Conquet, F., Steinmayr, M., Stratton, S. C., Porciatti, V. and Becker-André, M. (1998). Disruption of retinoid-related orphan receptor beta changes circadian behavior, causes retinal degeneration and leads to vacillans phenotype in mice. *EMBO J* **17**, 3867–3877.

Arribere, J. A., Bell, R. T., Fu, B. X. H., Artiles, K. L., Hartman, P. S. and Fire, A. Z. (2014). Efficient Marker-Free Recovery of Custom Genetic Modifications with CRISPR/Cas9 in *Caenorhabditis elegans*. *Genetics* **198**, 837–846.

Ashley, G., Duong, T., Levenson, M. T., Martinez, M. A. Q., Hibshman, J. D., Saeger, H. N., Doonan, R., Palmisano, N. J., Martinez-Mendez, R., Davidson, B., et al. (2020). Expanding the *Caenorhabditis elegans* auxin-inducible degron system toolkit with internal expression and degradation controls and improved modular constructs for CRISPR/Cas9-mediated genome editing. *bioRxiv* 10.1101/2020.05.12.090217

Barton, M. K. and Kimble, J. (1990). *fog-1*, a regulatory gene required for specification of spermatogenesis in the germ line of *Caenorhabditis elegans*. *Genetics* **125**, 29–39.

Barton, M. K., Schedl, T. B. and Kimble, J. (1987). Gain-of-function mutations of *fem-3*, a sex-determination gene in *Caenorhabditis elegans*. *Genetics* **115**, 107–119.

Beall, E. L., Lewis, P. W., Bell, M., Rocha, M., Jones, D. L. and Botchan, M. R. (2007). Discovery of tMAC: a *Drosophila* testis-specific meiotic arrest complex paralogous to Myb-Muv B. *Genes Dev* **21**, 904–919.

Bolcun-Filas, E., Bannister, L. A., Barash, A., Schimenti, K. J., Hartford, S. A., Eppig, J. J., Handel, M. A., Shen, L. and Schimenti, J. C. (2011). A-MYB (MYBL1) transcription factor is a master regulator of male meiosis. *Development* **138**, 3319–3330.

Chen, P. and Ellis, R. E. (2000). TRA-1A regulates transcription of *fog-3*, which controls germ cell fate in *C. elegans*. *Development* **127**, 3119–3129.

Chu, D. S. and Shakes, D. C. (2013). Spermatogenesis. In *Germ Cell Development in* C. elegans (ed. Schedl, T.), pp. 171–203. New York, NY: Springer New York.

Chung, S. S. W., Sung, W., Wang, X. and Wolgemuth, D. J. (2004). Retinoic acid receptor alpha is required for synchronization of spermatogenic cycles and its absence results in progressive breakdown of the spermatogenic process. *Dev Dyn* **230**, 754–766.

Church, D. L., Guan, K. L. and Lambie, E. J. (1995). Three genes of the MAP kinase cascade, *mek-2*, *mpk-1/sur-1* and *let-60 ras*, are required for meiotic cell cycle progression in *Caenorhabditis elegans*. *Development* **121**, 2525–2535.

del Castillo-Olivares, A., Kulkarni, M. and Smith, H. E. (2009). Regulation of sperm gene expression by the GATA factor ELT-1. *Dev Biol* **333**, 397–408.

Dernburg, A. F., Zalevsky, J., Colaiácovo, M. P. and Villeneuve, A. M. (2000). Transgene-mediated cosuppression in the *C. elegans* germ line. *Genes Dev* **14**, 1578–1583.

Dickinson, D. J., Pani, A. M., Heppert, J. K., Higgins, C. D. and Goldstein, B. (2015). Streamlined Genome Engineering with a Self-Excising Drug Selection Cassette. *Genetics* **200**, 1035–1049.

Dickinson, D. J., Slabodnick, M. M., Chen, A. H. and Goldstein, B. (2018). SapTrap assembly of repair templates for Cas9-triggered homologous recombination with a self-excising cassette. *microPublication Biology*. 10.17912/W2KT0N.

Drapek, C., Sparks, E. E. and Benfey, P. N. (2017). Uncovering Gene Regulatory Networks Controlling Plant Cell Differentiation. *Trends in Genetics* **33**, 529–539.

Ebbing, A., Vértesy, Á., Betist, M. C., Spanjaard, B., Junker, J. P., Berezikov, E., Van Oudenaarden, A. and Korswagen, H. C. (2018). Spatial Transcriptomics of *C. elegans* Males and Hermaphrodites Identifies Sex-Specific Differences in Gene Expression Patterns. *Dev Cell* **47**, 801-813.e6.

Edgar, L. G. (1995). Blastomere Culture and Analysis. In *Methods in Cell Biology* (ed. Epstein, H. F. and Shakes, D. C.), pp. 303–321. Academic Press.

Ellis, R. and Schedl, T. (2007). Sex determination in the germ line. *WormBook : the online review of C. elegans biology* 1–13.

Engert, C. G., Droste, R., Van Oudenaarden, A. and Horvitz, H. R. (2018). A *Caenorhabditis elegans* protein with a PRDM9-like SET domain localizes to chromatin-associated foci and promotes spermatocyte gene expression, sperm production and fertility. *PLoS Genet* **14**, e1007295.

Frand, A. R., Russel, S. and Ruvkun, G. (2005). Functional Genomic Analysis of *C. elegans* Molting. *PLoS Biol* **3**, e312.

Frøkjaer-Jensen, C., Davis, M. W., Hopkins, C. E., Newman, B. J., Thummel, J. M., Olesen, S.-P., Grunnet, M. and Jorgensen, E. M. (2008). Single-copy insertion of transgenes in *Caenorhabditis elegans*. *Nat Genet* **40**, 1375–1383.

Gely-Pernot, A., Raverdeau, M., Célébi, C., Dennefeld, C., Feret, B., Klopfenstein, M., Yoshida, S., Ghyselinck, N. B. and Mark, M. (2012). Spermatogonia differentiation requires retinoic acid receptor γ. *Endocrinology* **153**, 438–449.

Gely-Pernot, A., Raverdeau, M., Teletin, M., Vernet, N., Feret, B., Klopfenstein, M., Dennefeld, C., Davidson, I., Benoit, G., Mark, M., et al. (2015). Retinoic Acid Receptors Control Spermatogonia Cell-Fate and Induce Expression of the SALL4A Transcription Factor. *PLoS Genet* **11**, e1005501.

Gissendanner, C. R., Crossgrove, K., Kraus, K. A., Maina, C. V. and Sluder, A. E. (2004). Expression and function of conserved nuclear receptor genes in *Caenorhabditis elegans*. *Dev Biol* **266**, 399–416.

Golden, A., Sadler, P. L., Wallenfang, M. R., Schumacher, J. M., Hamill, D. R., Bates, G., Bowerman, B., Seydoux, G. and Shakes, D. C. (2000). Metaphase to anaphase (*mat*) transition-defective mutants in *Caenorhabditis elegans*. *J Cell Biol* **151**, 1469–1482.

Hendriks, G.-J., Gaidatzis, D., Aeschimann, F. and Großhans, H. (2014). Extensive oscillatory gene expression during *C. elegans* larval development. *Mol Cell* **53**, 380–392.

Hodgkin, J. (1987). A genetic analysis of the sex-determining gene, *tra-1*, in the nematode *Caenorhabditis elegans*. *Genes Dev* **1**, 731–745.

Horvath, G. C., Kistler, M. K. and Kistler, W. S. (2009). RFX2 is a candidate downstream amplifier of A-MYB regulation in mouse spermatogenesis. *BMC Developmental Biology* **9**, 63.

Hsu, J.-Y., Sun, Z.-W., Li, X., Reuben, M., Tatchell, K., Bishop, D. K., Grushcow, J. M., Brame, C. J., Caldwell, J. A., Hunt, D. F., et al. (2000). Mitotic Phosphorylation of Histone H3 Is Governed by Ipl1/aurora Kinase and Glc7/PP1 Phosphatase in Budding Yeast and Nematodes. *Cell* **102**, 279–291.

Hu, J., Cheng, S., Wang, H., Li, X., Liu, S., Wu, M., Liu, Y. and Wang, X. (2019). Distinct roles of two myosins in *C. elegans* spermatid differentiation. *PLoS Biol* **17**, e3000211-31.

Jin, S.-W., Kimble, J. and Ellis, R. E. (2001). Regulation of Cell Fate in *Caenorhabditis elegans* by a Novel Cytoplasmic Polyadenylation Element Binding Protein. *Developmental Biology* **229**, 537–553.

Kageyama, Y., Masuda, S., Hirose, S. and Ueda, H. (1997). Temporal regulation of the mid-prepupal gene FTZ-F1: DHR3 early late gene product is one of the plural positive regulators. *Genes Cells* **2**, 559–569.

Kallen, J. A., Schlaeppi, J.-M., Bitsch, F., Geisse, S., Geiser, M., Delhon, I. and Fournier, B. (2002). X-Ray Structure of the hRORα LBD at 1.63 Å: Structural and Functional Data that Cholesterol or a Cholesterol Derivative Is the Natural Ligand of RORα. *Structure* **10**, 1697–1707.

Kallen, J., Schlaeppi, J.-M., Bitsch, F., Delhon, I. and Fournier, B. (2004). Crystal structure of the human RORalpha Ligand binding domain in complex with cholesterol sulfate at 2.2 A. *J Biol Chem* **279**, 14033–14038.

Kang, T.-H., Lindsey-Boltz, L. A., Reardon, J. T. and Sancar, A. (2010). Circadian control of XPA and excision repair of cisplatin-DNA damage by cryptochrome and HERC2 ubiquitin ligase. *Proceedings of the National Academy of Sciences* **107**, 4890–4895.

Kasimatis, K. R., Moerdyk-Schauwecker, M. J. and Phillips, P. C. (2018). Auxin-Mediated Sterility Induction System for Longevity and Mating Studies in *Caenorhabditis elegans*. *G3 (Bethesda)* **8**, 2655–2662.

Kelly, W. G., Schaner, C. E., Dernburg, A. F., Lee, M.-H., Kim, S. K., Villeneuve, A. M. and Reinke, V. (2002). X-chromosome silencing in the germline of *C. elegans*. *Development* **129**, 479–492.

Kennaway, D. J., Boden, M. J. and Varcoe, T. J. (2012). Circadian rhythms and fertility. *Molecular and Cellular Endocrinology* **349**, 56–61.

Kosinski, M. (2005). *C. elegans* sperm bud vesicles to deliver a meiotic maturation signal to distant oocytes. *Development* **132**, 3357–3369.

Kostrouchova, M., Krause, M., Kostrouch, Z. and Rall, J. E. (1998). CHR3: a *Caenorhabditis elegans* orphan nuclear hormone receptor required for proper epidermal development and molting. *Development* **125**, 1617–1626.

Kostrouchova, M., Krause, M., Kostrouch, Z. and Rall, J. E. (2001). Nuclear hormone receptor CHR3 is a critical regulator of all four larval molts of the nematode *Caenorhabditis elegans*. *Proc Natl Acad Sci USA* **98**, 7360–7365.

Kouns, N. A., Nakielna, J., Behensky, F., Krause, M. W., Kostrouch, Z. and Kostrouchova, M. (2011). NHR-23 dependent collagen and hedgehog-related genes required for molting. *Biochemical and Biophysical Research Communications* **413**, 515–520.

Kulkarni, M., Shakes, D. C., Guevel, K. and Smith, H. E. (2012). SPE-44 implements sperm cell fate. *PLoS Genet* **8**, e1002678.

Laktionov, P. P., Maksimov, D. A., Romanov, S. E., Antoshina, P. A., Posukh, O. V., White-Cooper, H., Koryakov, D. E. and Belyakin, S. N. (2018). Genome-wide analysis of gene regulation mechanisms during *Drosophila* spermatogenesis. *Epigenetics & Chromatin* **11**, 1–15.

Lam, G. T., Jiang, C. and Thummel, C. S. (1997). Coordination of larval and prepupal gene expression by the DHR3 orphan receptor during Drosophila metamorphosis. *Development* **124**, 1757–1769.

Lamitina, S. T. and L'Hernault, S. W. (2002). Dominant mutations in the *Caenorhabditis elegans* Myt1 ortholog *wee-1.3* reveal a novel domain that controls M-phase entry during spermatogenesis. *Development* **129**, 5009–5018.

Levine, M. and Davidson, E. H. (2005). Gene regulatory networks for development. *PNAS* **102**, 4936–4942.

L'Hernault, S. W. and Arduengo, P. M. (1992). Mutation of a putative sperm membrane protein in *Caenorhabditis elegans* prevents sperm differentiation but not its associated meiotic divisions. *The Journal of Cell Biology* **119**, 55–68.

L'Hernault, S. W., Shakes, D. C. and Ward, S. (1988). Developmental genetics of chromosome I spermatogenesis-defective mutants in the nematode *Caenorhabditis elegans*. *Genetics* **120**, 435–452.

Li, X. Z., Roy, C. K., Dong, X., Bolcun-Filas, E., Wang, J., Han, B. W., Xu, J., Moore, M. J., Schimenti, J. C., Weng, Z., et al. (2013). An Ancient Transcription Factor Initiates the Burst of piRNA Production during Early Meiosis in Mouse Testes. *Molecular Cell* **50**, 67–81.

Machaca, K. and L'Hernault, S. W. (1997). The *Caenorhabditis elegans spe-5* gene is required for morphogenesis of a sperm-specific organelle and is associated with an inherent cold-sensitive phenotype. *Genetics* **146**, 567–581.

Macneil, L. T., Watson, E., Arda, H. E., Zhu, L. J. and Walhout, A. J. M. (2013). Diet-Induced Developmental Acceleration Independent of TOR and Insulin in *C. elegans*. *Cell* **153**, 240–252.

Mandal, K., Sarkar, R. K., Sen Sharma, S., Jain, A. and Majumdar, S. S. (2018). Sertoli cell specific knockdown of RAR-related orphan receptor (ROR) alpha at puberty reduces sperm count in rats. *Gene* **641**, 18–24.

McKearin, D. M. and Spradling, A. C. (1990). *bag-of-marbles*: a *Drosophila* gene required to initiate both male and female gametogenesis. *Genes Dev* **4**, 2242–2251.

Medwig-Kinney, T. N., Smith, J. J., Palmisano, N. J., Tank, S., Zhang, W. and Matus, D. Q. (2020). A developmental gene regulatory network for *C. elegans* anchor cell invasion. *Development* **147**, dev185850

Merritt, C., Rasoloson, D., Ko, D. and Seydoux, G. (2008). 3' UTRs are the primary regulators of gene expression in the *C. elegans* germline. *Curr Biol* **18**, 1476–1482.

Metcalf, C. E. and Wassarman, D. A. (2007). Nucleolar colocalization of TAF1 and testis-specific TAFs during *Drosophila* spermatogenesis. *Dev Dyn* **236**, 2836–2843.

Miller, M. A., Nguyen, V. Q., Lee, M.-H., Kosinski, M., Schedl, T., Caprioli, R. M. and Greenstein, D. (2001). A sperm cytoskeletal protein that signals oocyte meiotic maturation and ovulation. *Science* **291**, 2144–2147.

Minniti, A. N., Sadler, C. and Ward, S. (1996). Genetic and molecular analysis of *spe-27*, a gene required for spermiogenesis in *Caenorhabditis elegans* hermaphrodites. *Genetics* **143**, 213–223.

Morse, D., Cermakian, N., Brancorsini, S., Parvinen, M. and Sassone-Corsi, P. (2003). No circadian rhythms in testis: Period1 expression is clock independent and developmentally regulated in the mouse. *Molecular Endocrinology* **17**, 141–151.

Muhlrad, P. J. and Ward, S. (2002). Spermiogenesis initiation in *Caenorhabditis elegans* involves a casein kinase 1 encoded by the *spe-6* gene. *Genetics* **161**, 143–155.

Nance, J., Minniti, A. N., Sadler, C. and Ward, S. (1999). *spe-12* encodes a sperm cell surface protein that promotes spermiogenesis in *Caenorhabditis elegans*. *Genetics* **152**, 209–220.

Nance, J., Davis, E. B. and Ward, S. (2000). *spe-29* encodes a small predicted membrane protein required for the initiation of sperm activation in *Caenorhabditis elegans*. *Genetics* **156**, 1623–1633.

Nishimura, H. and L'Hernault, S. W. (2010). Spermatogenesis-defective (*spe*) mutants of the nematode *Caenorhabditis elegans* provide clues to solve the puzzle of male germline functions during reproduction. *Dev Dyn* **239**, 1502–1514.

Nishimura, K., Fukagawa, T., Takisawa, H., Kakimoto, T. and Kanemaki, M. (2009). An auxin-based degron system for the rapid depletion of proteins in nonplant cells. *Nat Meth* **6**, 917–922.

Okamoto, H. and Thomson, J. N. (1985). Monoclonal antibodies which distinguish certain classes of neuronal and supporting cells in the nervous tissue of the nematode *Caenorhabditis elegans*. *J Neurosci* **5**, 643–653.

Page, B. D., Zhang, W., Steward, K., Blumenthal, T. and Priess, J. R. (1997). ELT-1, a GATA-like transcription factor, is required for epidermal cell fates in *Caenorhabditis elegans* embryos. *Genes Dev.* **11**, 1651–1661.

Paix, A., Folkmann, A., Rasoloson, D. and Seydoux, G. (2015). High Efficiency, Homology-Directed Genome Editing in *Caenorhabditis elegans* Using CRISPR-Cas9 Ribonucleoprotein Complexes. *Genetics* **201**, 47–54.

Patel, R. and Frand, A. R. (2018). A Regulatory Loop between the Retinoid-Related Orphan Nuclear Receptor NHR-23 and *let-7* family microRNAs Modulates the *C. elegans* Molting Cycle. *bioRxiv* 10.1101/506261

Reinke, V., Gil, I. S., Ward, S. and Kazmer, K. (2004). Genome-wide germline-enriched and sex-biased expression profiles in *Caenorhabditis elegans*. *Development (Cambridge, England)* **131**, 311–323.

Roach, N. P., Sadowski, N., Alessi, A. F., Timp, W., Taylor, J. and Kim, J. K. (2020). The full-length transcriptome of *C. elegans* using direct RNA sequencing. *Genome Res.*

Sadler, P. L. and Shakes, D. C. (2000). Anucleate *Caenorhabditis elegans* sperm can crawl, fertilize oocytes and direct anterior-posterior polarization of the 1-cell embryo. *Development* **127**, 355–366.

Sato, T. K., Panda, S., Miraglia, L. J., Reyes, T. M., Rudic, R. D., McNamara, P., Naik, K. A., FitzGerald, G. A., Kay, S. A. and Hogenesch, J. B. (2004). A functional genomics strategy reveals Rora as a component of the mammalian circadian clock. *Neuron* **43**, 527–537.

Schedl, T., Graham, P. L., Barton, M. K. and Kimble, J. (1989). Analysis of the role of *tra-1* in germline sex determination in the nematode *Caenorhabditis elegans*. *Genetics* **123**, 755–769.

Schubert, C. M., Lin, R., de Vries, C. J., Plasterk, R. H. and Priess, J. R. (2000). MEX-5 and MEX-6 function to establish soma/germline asymmetry in early *C. elegans* embryos. *Mol Cell* **5**, 671–682.

Schwartz, M. L. and Jorgensen, E. M. (2016). SapTrap, a Toolkit for High-Throughput CRISPR/Cas9 Gene Modification in *Caenorhabditis elegans*. *Genetics* **202**, 1277–1288.

Seidel, H. S., Rockman, M. V. and Kruglyak, L. (2008). Widespread genetic incompatibility in *C. elegans* maintained by balancing selection. *Science* **319**, 589–594.

Shakes, D. C. and Ward, S. (1989). Initiation of spermiogenesis in *C. elegans*: a pharmacological and genetic analysis. *Dev Biol* **134**, 189–200.

Shakes, D. C., Wu, J.-C., Sadler, P. L., Laprade, K., Moore, L. L., Noritake, A. and Chu, D. S. (2009). Spermatogenesis-specific features of the meiotic program in *Caenorhabditis elegans*. *PLoS Genet* **5**, e1000611.

Soroosh, P., Wu, J., Xue, X., Song, J., Sutton, S. W., Sablad, M., Yu, J., Nelen, M. I., Liu, X., Castro, G., et al. (2014). Oxysterols are agonist ligands of RORγt and drive Th17 cell differentiation. *Proceedings of the National Academy of Sciences* **111**, 12163–12168.

Subramaniam, K. and Seydoux, G. (2003). Dedifferentiation of primary spermatocytes into germ cell tumors in *C. elegans* lacking the Pumilio-like protein PUF-8. *Current Biology* **13**, 134–139.

Tzur, Y. B., Winter, E., Gao, J., Hashimshony, T., Yanai, I. and Colaiácovo, M. P. (2018). Spatiotemporal Gene Expression Analysis of the *Caenorhabditis elegans* Germline Uncovers a Syncytial Expression Switch. *Genetics* **210**, 587–605.

Varkey, J. P., Jansma, P. L., Minniti, A. N. and Ward, S. (1993). The *Caenorhabditis elegans spe-6* gene is required for major sperm protein assembly and shows second site non-complementation with an unlinked deficiency. *Genetics* **133**, 79–86.

Wang, Y., Kumar, N., Crumbley, C., Griffin, P. R. and Burris, T. P. (2010). A second class of nuclear receptors for oxysterols: Regulation of RORalpha and RORgamma activity by 24S-hydroxycholesterol (cerebrosterol). *Biochim Biophys Acta* **1801**, 917–923.

Ward, J. D. (2015). Rapid and Precise Engineering of the *Caenorhabditis elegans* Genome with Lethal Mutation Co-Conversion and Inactivation of NHEJ Repair. *Genetics* **199**, 363–377.

Ward, S., Argon, Y. and Nelson, G. A. (1981). Sperm morphogenesis in wild-type and fertilization-defective mutants of *Caenorhabditis elegans*. *The Journal of Cell Biology* **91**, 26–44.

White, K. P., Hurban, P., Watanabe, T. and Hogness, D. S. (1997). Coordination of Drosophila metamorphosis by two ecdysone-induced nuclear receptors. *Science* **276**, 114–117.

White-Cooper, H. and Bausek, N. (2010). Evolution and spermatogenesis. *Philos. Trans. R. Soc. Lond., B, Biol. Sci.* **365**, 1465–1480.

Winter, E. S., Schwarz, A., Fabig, G., Feldman, J. L., Pires-daSilva, A., Müller-Reichert, T., Sadler, P. L. and Shakes, D. C. (2017). Cytoskeletal variations in an asymmetric cell division support diversity in nematode sperm size and sex ratios. *Development* **144**, 3253–3263.

Zarkower, D. and Hodgkin, J. (1992). Molecular analysis of the *C. elegans* sex-determining gene *tra-1*: a gene encoding two zinc finger proteins. *Cell* **70**, 237–249.

Zhang, L., Ward, J. D., Cheng, Z. and Dernburg, A. F. (2015). The auxin-inducible degradation (AID) system enables versatile conditional protein depletion in *C. elegans*. *Development* **142**, 4374–4384.

Zhang, D., Xie, D., Lin, X., Ma, L., Chen, J., Zhang, D., Wang, Y., Duo, S., Feng, Y., Zheng, C., et al. (2018). The transcription factor SOX30 is a key regulator of mouse spermiogenesis. *Development* **145**, dev164723-11.

Zhu, G.-D. and L'Hernault, S. W. (2003). The *Caenorhabditis elegans spe-39* gene is required for intracellular membrane reorganization during spermatogenesis. *Genetics* **165**, 145–157.

Figures

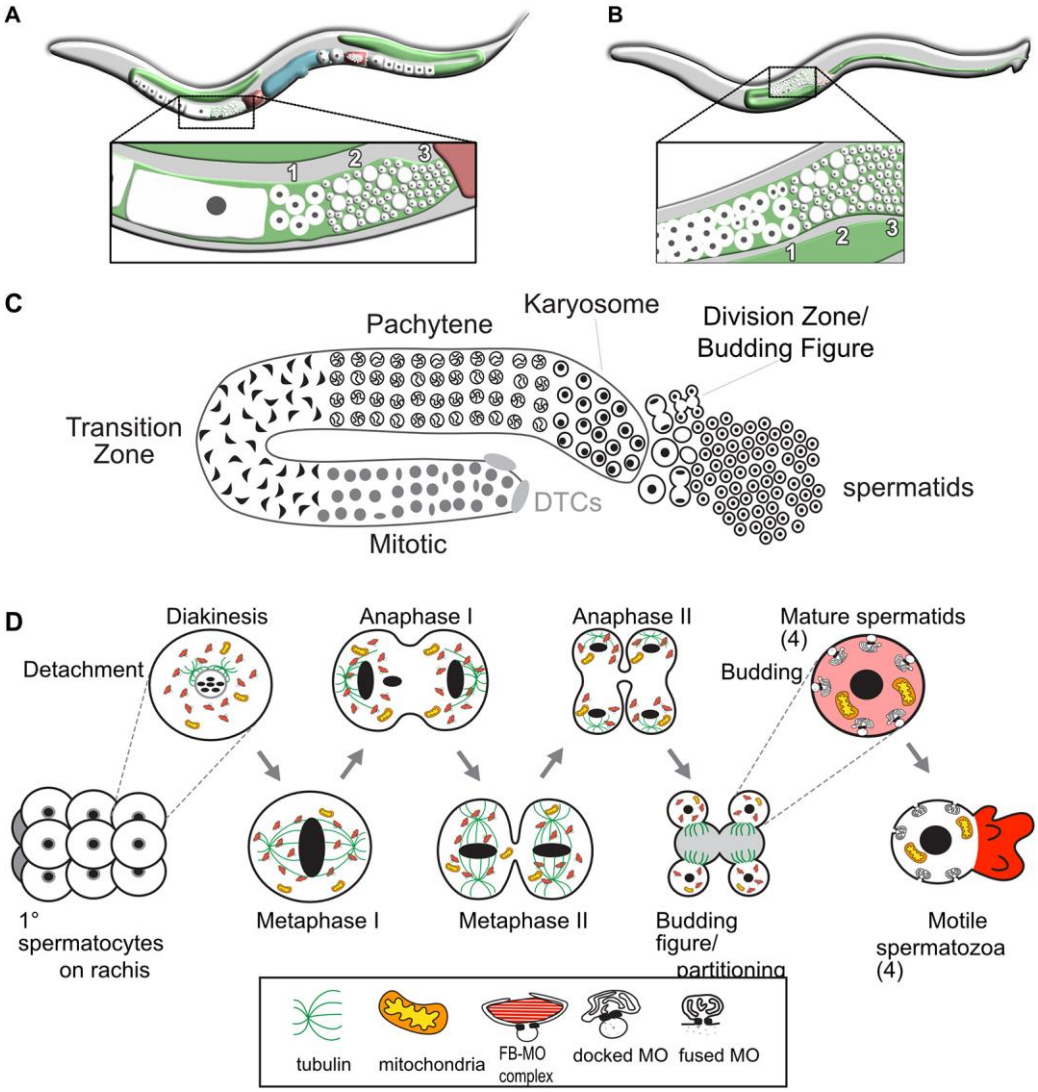

Fig. 1. Overview of *C. elegans* spermatogenesis. (A,B) Cartoons depicting a young adult *C. elegans* hermaphrodite and male and their respective germlines. The hermaphrodite germline (A) is transitioning from spermatogenesis to oogenesis. The enlarged views highlight the linear arrangement of the primary spermatocytes (1), residual bodies (RB) (2), and mature haploid spermatids (3). (C) Stylized cartoon of a surface view of the male germline highlighting its overall linear organization. Mitotic proliferation of the germline stem cells is maintained by two somatic distal tip cells (DTCs) which form the germ cell niche. The early events of meiotic prophase including homolog pairing and formation of the synaptonemal complex, occur in the transition zone. Following an extended pachytene stage, spermatocytes enter a karyosome stage before mature spermatocytes detach from the syncytial germline and divide

meiotically. The first meiotic division is often incomplete, leaving secondary spermatocytes linked by a cytoplasmic connection. Following anaphase II, the spermatocytes morph into budding figures that split into residual bodies and haploid spermatids. (D) Details of the meiotic divisions and post-meiotic partitioning event. Once spermatocytes detach from the germline syncytium, they pass through a brief diakinesis stage before undergoing nuclear envelope breakdown and initiating meiotic divisions. During the post-meiotic partitioning event, microtubules become acentrosomal and localize to the developing residual body (Winter et al., 2017). Components retained in the spermatids include fibrous body-membranous organelles (FB-MO), mitochondria, chromatin, and centrioles. Components discarded within the RB include the cell's tubulin, actin, ER, and ribosomes; mature sperm are thus both transcriptionally and translationally inactive. Following separation from the RB, FBs disassemble and release unpolymerized MSP and the MOs dock with the plasma membrane. Males store sperm in this inactive spermatid state. During spermatid activation, MOs fuse with the plasma membrane and unpolymerized MSP localizes to the pseudopod where it forms fibers that are required for spermatozoon motility.

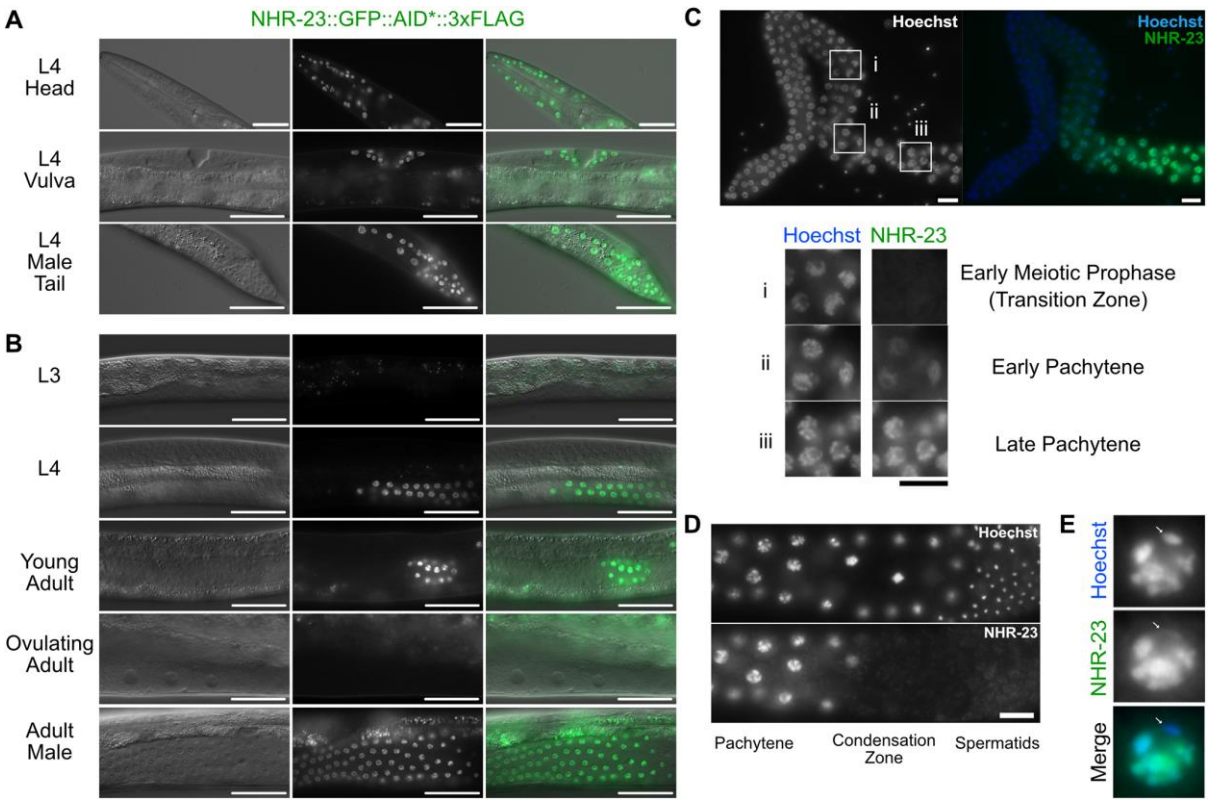

Fig. 2. NHR-23::GFP::AID*::3xFLAG is expressed in somatic cells throughout development and in spermatogenic germlines. A strain carrying GFP::AID*::3xFLAG knocked-in to the endogenous *nhr-23* gene to produce a C-terminal translational fusion to all known *nhr-23* isoforms was used to monitor endogenous NHR-23 expression. (A) Representative DIC and GFP images of NHR-23::GFP::AID*::3xFLAG L4 larvae, specifically hypodermal cells of a hermaphrodite head, vulval precursor cells, and seam/hypodermal cells of the male tail. (B) Representative DIC and GFP images of NHR-23::GFP::AID*::3xFLAG in pachytene cells of the germline in L3, L4, young adult, ovulating adult and adult male worms. (C) Fluorescent images of NHR-23::GFP::AID*::3xFLAG in a dissected adult male germline. Inset boxes show cells in early meiotic prophase (transition zone) (i), early (ii) and late (iii) pachytene. (D) Representative fluorescent images of NHR-23::GFP::AID*::3xFLAG in a late pachytene male germline. (E) Representative image of a late pachytene nucleus expressing NHR-23::GFP::AID*::3xFLAG. The location of the X chromosome is noted with a white arrow. Scale bars: (A, B) 40 µm, (C-E) 10 µm. A minimum of 12 P0 animals were analyzed in A, B, and C . Nuclei were visualized by Hoechst stain in C-E.

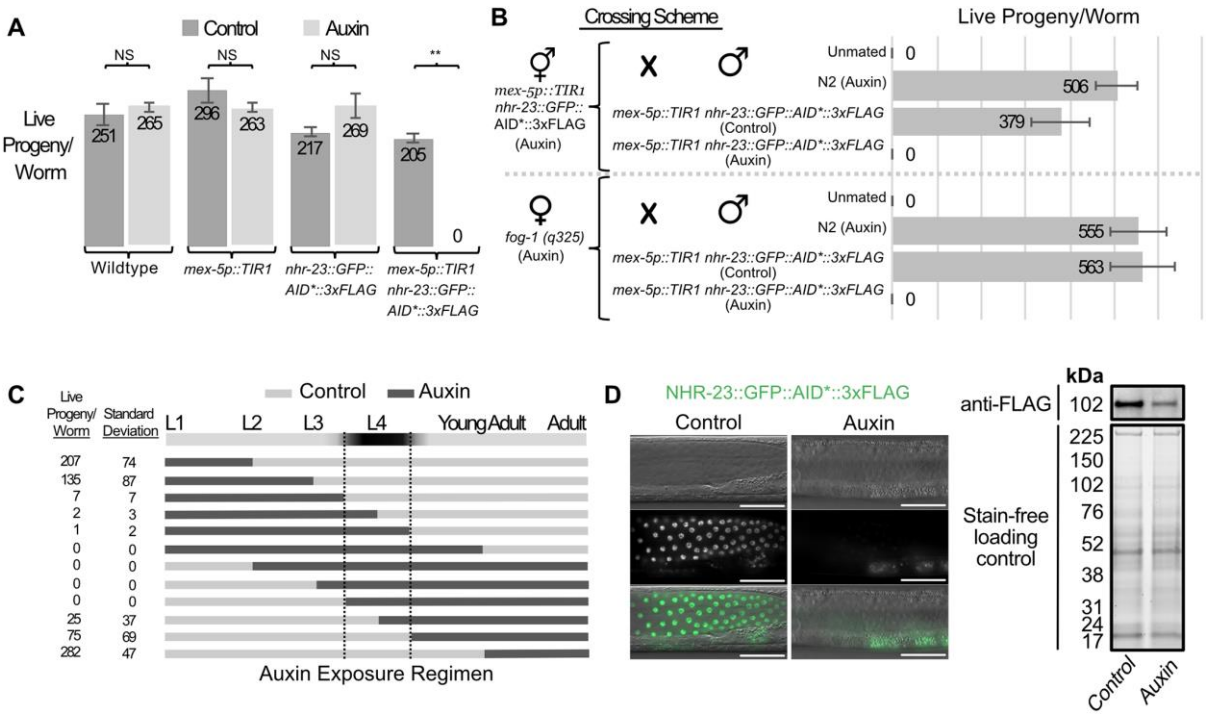

Fig. 3. NHR-23-depletion in the germline during periods of spermatogenesis causes infertility in hermaphrodites and males. (A) Average number of live progeny produced by wildtype, *mex-5p::TIR1, nhr-23::GFP::AID*::3xFLAG* or *mex-5p::TIR1 nhr-23::GFP::AID*::3xFLAG* hermaphrodites grown from L1 through adulthood on MYOB media with or without 4 mM auxin. A Student's t-test was performed for each genotype comparing brood sizes on control media versus 4 mM auxin. A p-value greater than 0.01 was considered non-significant (NS). The **denotes p<0.00001. n=12 for each brood size. (B) Average number of live progeny produced by *mex-5p::TIR1 nhr-23::GFP::AID*::3xFLAG* or *fog-1(q325)* hermaphrodites grown from L1 on MYOB media with 4 mM auxin. Hermaphrodites were either unmated or crossed to males of the indicated genotype; males were grown from L1 to adulthood on control or 4 mM auxin media. (n=12) (C) Average number of live progeny produced by *mex-5p::TIR1 nhr-23::GFP::AID*::3xFLAG* hermaphrodites shifted on or off 4 mM auxin at different points in development. Dark horizontal bands represent growth on media with 4 mM auxin and light horizontal bands represent growth on control media lacking auxin. n=12 for each condition. (D) DIC and fluorescent images of *mex-5p::TIR1 nhr-23::GFP::AID*::3xFLAG* adult male germlines after animals were grown from L1 on MYOB media ±4 mM auxin. NHR-23-depletion results in minimally detectable GFP signal by fluorescence microscopy, but FLAG signal remains detectable in western

blots. Scale bars: 40um. Anti-FLAG immunoblot analyses of lysates are from synchronized male *mex-5p::TIR1 nhr-23::GFP::AID*::3xFLAG* animals grown on control or 4 mM auxin media. Marker size (in kilodaltons) is provided. Predicted size of the fusion protein is 98.7 kDa, based on the NHR-23 isoform expressed in adults in a Nanopore direct RNA sequencing dataset (Roach et al., 2020). Stain-free (Bio-Rad) analysis, which visualizes total protein on the membrane is provided as a loading control.

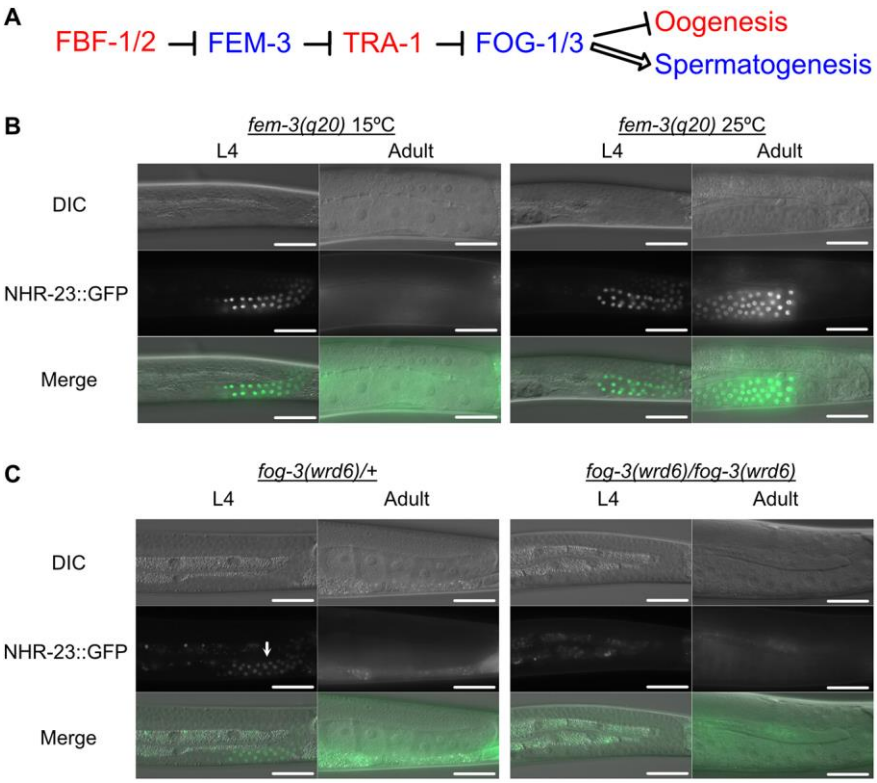

Fig. 4. *nhr-23* is downstream of the germline sex determination pathway. (A) Simplified schematic of the *C. elegans* sex determination pathway and their effect on gamete fate. The wildtype function of the factors in blue text is to promote spermatogenesis, while the factors in red promote oogenesis. (B) DIC and GFP images of *mex-5p::TIR1 nhr-23::GFP::AID*::3xFLAG*; *fem-3(q20)* L4 and adult hermaphrodites grown from L1 onwards at permissive (15°C) or restrictive (25°C) temperatures. (C) DIC and GFP images of *mex-5p::TIR1 nhr-23::GFP::AID*::3xFLAG; fog-3(wrd6)* L4 and adult hermaphrodites. The white arrow indicates NHR-23::GFP::AID*::3xFLAG expression in late pachytene cells of a *fog-3(wrd6)* heterozygous hermaphrodite germline. Scale bars: 40 µm.

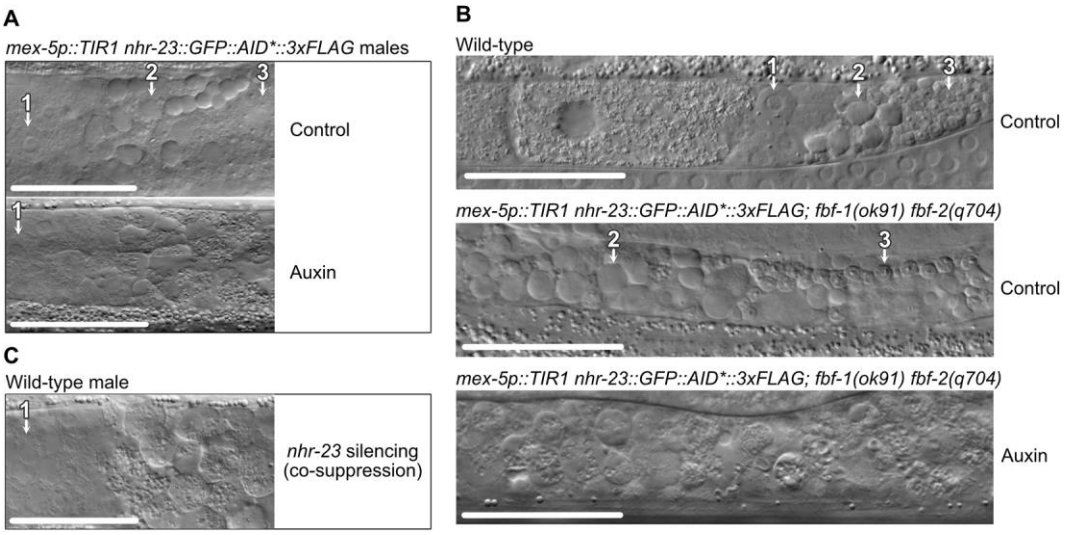

Fig. 5. NHR-23 is necessary for sperm development. (A) DIC images of the proximal germlines of *mex-5p::TIR1, nhr-23::GFP::AID*::3xFLAG* young adult males grown from L1 onwards on control or 4 mM auxin media. (B) DIC images of wild type and masculinized *mex-5p::TIR1, nhr-23::GFP::AID*::3xFLAG; fbf-1(ok91) fbf-2(q704)* hermaphrodites grown from L1 onwards on control or 4 mM auxin media. Primary spermatocytes (1) have a flat morphology with a large nucleus. Residual bodies (2) appear as highly refractile raised button-like structures. Spermatids (3) are readily discernible through their characteristic small refractive nuclei. (C) DIC image of the proximal germline in a wildtype young adult male F1 progeny from a P_0 animal injected with a *mex-5p::nhr-23 cDNA* co-suppression construct, which promotes an RNAi-like depletion of targeted mRNA. Scale bars: 40 µm.

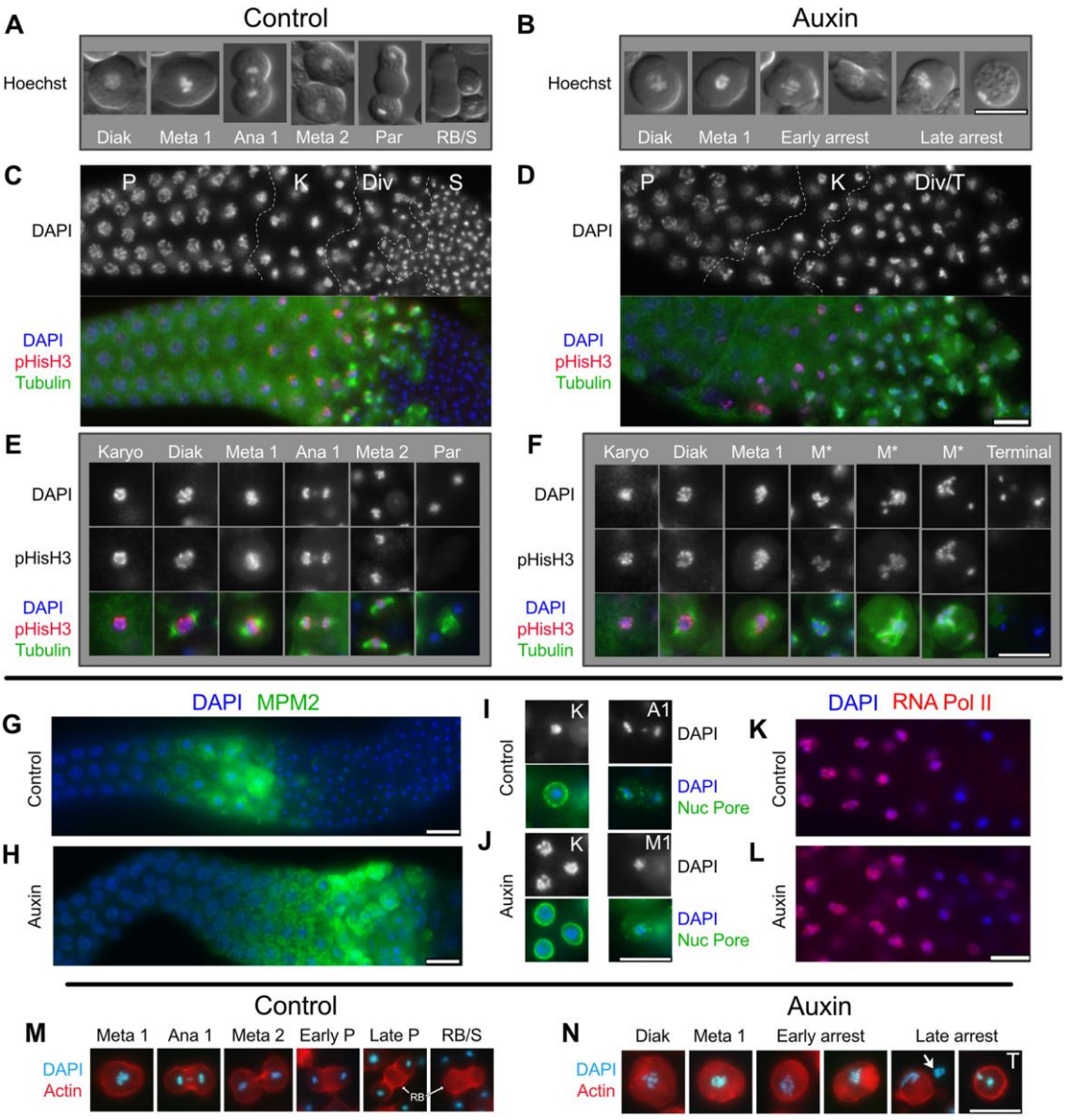

Figure 6. Metaphase I like arrest in NHR-23-depleted spermatocytes. (A,B) Live spermatocytes ordered according to stage. Differential interference contrast (DIC) images of cells were overlaid by epifluorescence images of their Hoechst stained nuclei. (C-J) Isolated and fixed male gonads and individual spermatocytes labeled with DAPI (blue) and indicated antibodies. (C,D) Gonad images show the proximal gonad from late pachytene (P) to either haploid spermatids (S) or terminal arrest (T) co-labelled with antibodies against α-tubulin (green) and phosphorylated histone H3 (ser10) (red). Controls (*nhr-23*::degron without auxin or *him-5* with auxin) on left, and *nhr-23*::degron with auxin on right. (E-F) Higher magnification images of individual spermatocytes. (G-H) Isolated control and NHR-23-depleted proximal male gonads

(pachytene and later meiotic stages) co-labelled with antibodies against MPM2 (green) which binds diverse mitotic and meiotic phosphorylated proteins. (I-J) Staged spermatocytes co-labelled with anti-nuclear pore protein (green) in control and NHR-23-depleted males. (K-L) Control and NHR-23-depleted gonads (pachytene through karyosome) co-labelled with anti-phospho-RNA polymerase II CTD repeat (red) shows turn-off of global transcription in karyosome spermatocytes. (M-N) Aldehyde fixed and staged spermatocytes with DNA pseudo-colored in cyan (DAPI) and actin microfilaments labeled with rhodamine-phalloidin (red). The arrow in the late arrested image shows chromatin from a lysed spermatocyte. Abbreviations: Pachytene (P), Karyosome (K), Meiotic Divisions (Div), Diakinesis (Diak), Metaphase I (Meta 1, MI), Aberrant Metaphase I (M*), Anaphase I (Ana 1, AI), Metaphase II (Meta 2), Post-meiotic Partitioning (Par), Residual Body (RB), Haploid Spermatids (S), Terminal-stage Spermatocyte (T). Scale bars: 10 μm.

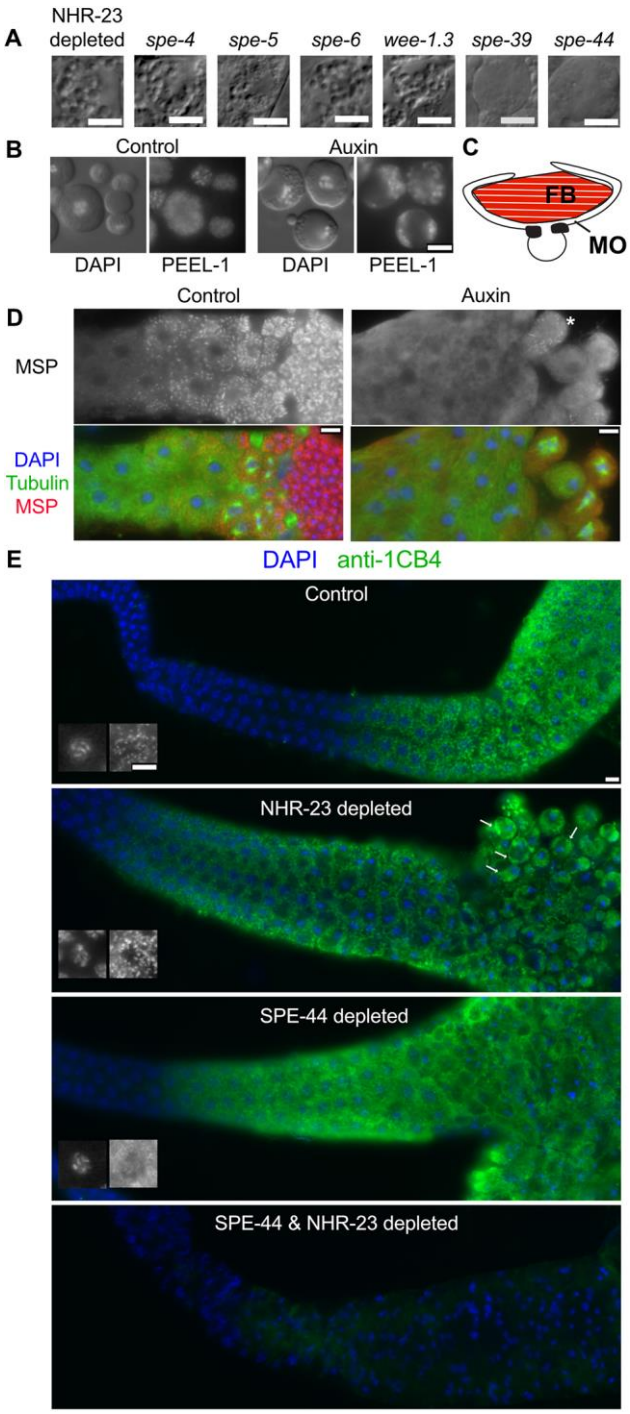

Figure 7. FB-MO defects in NHR-23 spermatocytes and synergy with SPE-44. (A) DIC images of arrested spermatocytes from spermatogenesis-defective mutants. (B) Control and NHR-23-depleted spermatocytes visualized by DIC/Hoechst (left) and the MO marker PEEL::GFP (right). (C) Schematic of an FB-MO complex showing an MSP-enriched fibrous body (FB) enveloped within arm-like extensions of the Golgi-derived membranous organelle (MO). (D) Proximal gonads from control and

NHR-23-depleted males co-labelled with DAPI and antibodies against tubulin and MSP. Asterisk indicates a single spermatocyte in the NHR-23-depleted gonad with MSP polymers. (E) Gonads from animals with indicated protein depletions co-labelled with DAPI and the anti-MO antibody 1CB4. Black and white images at the lower left of the E panels show DAPI (left) and 1CB4-stained MOs (right) in pachytene stage spermatocytes and highlight defects in SPE-44 spermatocytes. Arrows indicate clumping of 1CB4-stained bodies following NHR-23 depletion. Scale bars: 5 μm.

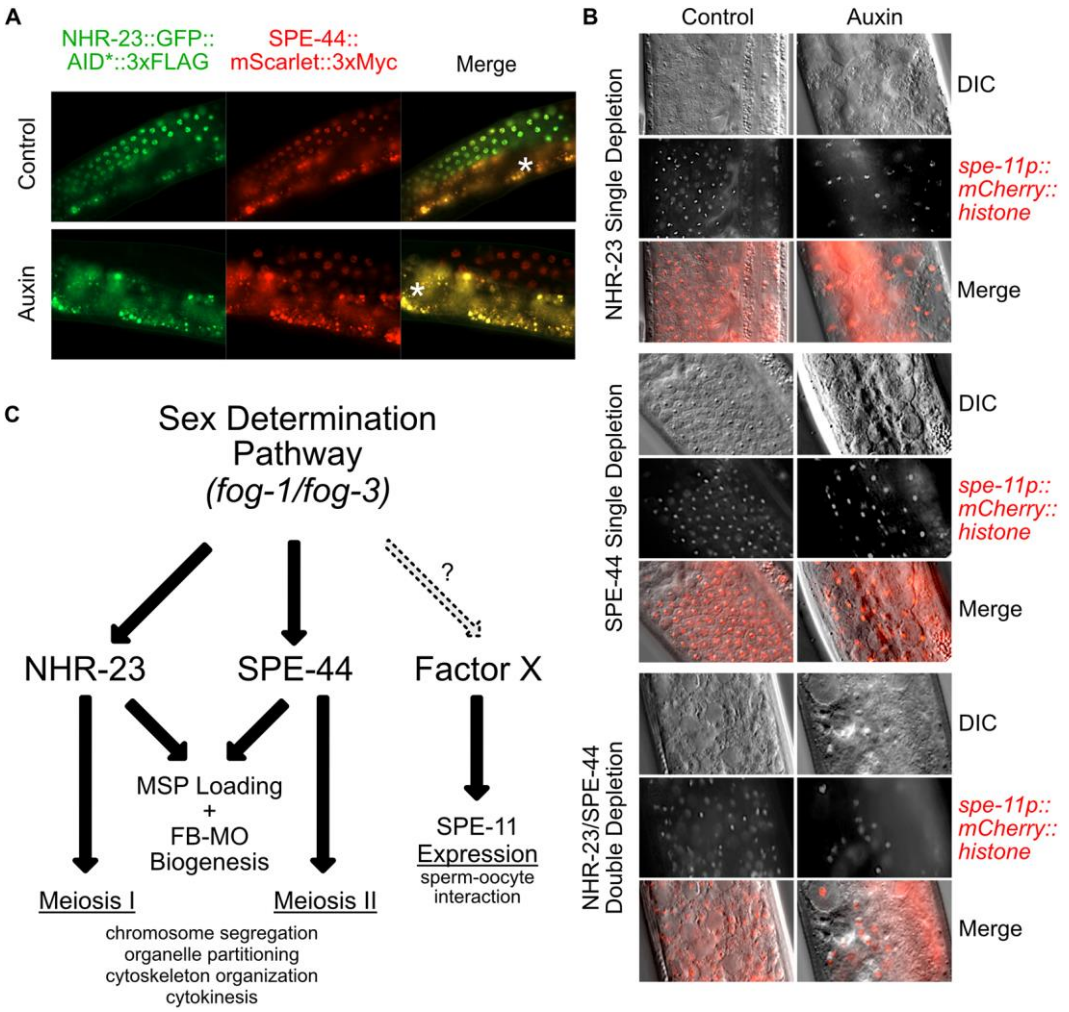

Fig. 8. Control of transcription in spermatogenesis is facilitated by multiple factors with divergent targets. (A) Fluorescent images of NHR-23::GFP::AID*::3xFLAG and *spe-44::mScarlet::3xMyc*. Worms containing both translational fusions as well as the *mex-5p::TIR1* driver were grown from L1 onwards on control or 4 mM auxin media. The asterisks indicate gut autofluorescence. (B) Representative DIC and fluorescent images of *spe-11p::mCherry::H2B* in adult males expressing *mex-5p::TIR1* in the germline. Worms individually expressed NHR-23::AID*::3xFLAG or SPE-44::AID*::3xFLAG or both and were grown from L1 until the young adult stage on control or 4 mM auxin media. (C) Model depicting the coordinated control of gene expression prior to and during the stages of spermatogenesis. NHR-23 and SPE-44 control distinct sets of genes to promote the events of meiosis I and II, respectively. They redundantly promote MSP loading and FB-MO biogenesis. A third pathway controlled by yet unidentified factors promotes the expression of genes involved in the sperm-oocyte interaction, such as *spe-11*.

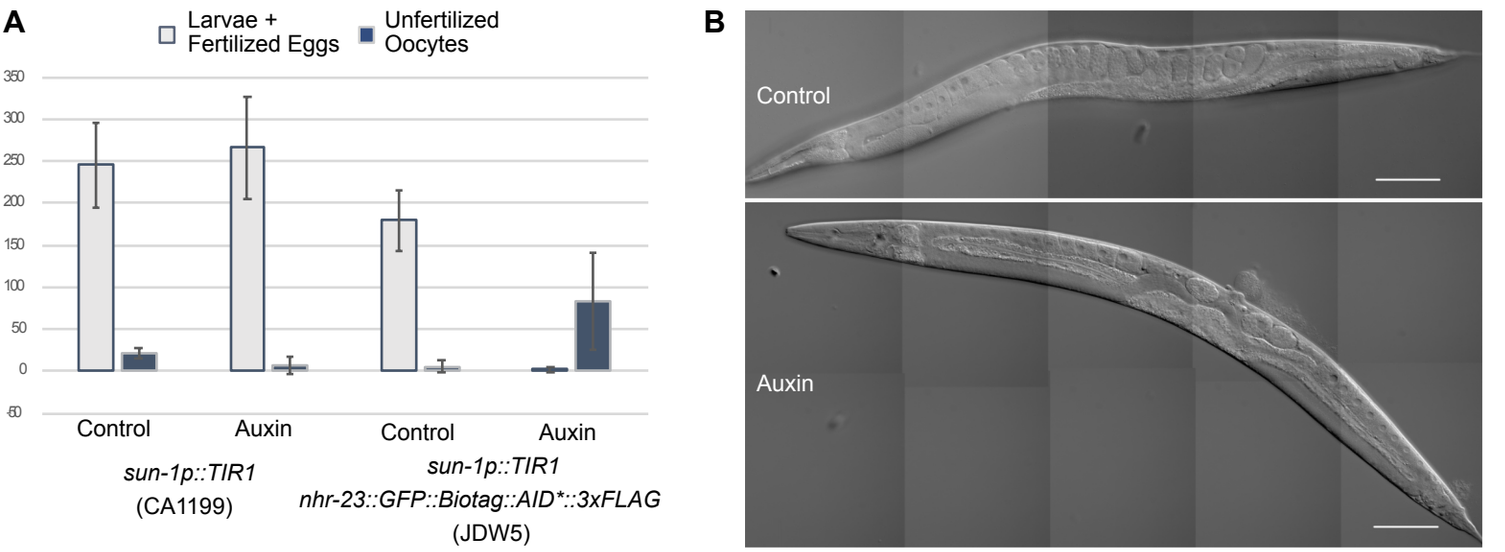

Fig. S1. NHR-23-depletion in worms expressing TIR1 from a *sun-1* promoter causes sterility similar to that observed when TIR1 is expressed from the *mex-5* promoter. (A) Combined count of L1 larvae/fertilized egg progeny or unfertilized oocyte from hermaphrodites grown from L1 onwards with or without 4 mM auxin. Error bars=standard deviation (n=12 for each condition) (B) Representative DIC images of L4 + 1 day *nhr-23::GFP::Biotag::AID*::3xFLAG; sun-1p::TIR1* hermaphrodites in the absence (top) or presence (bottom) of 4 mM auxin. Scale bars: 80 µm.

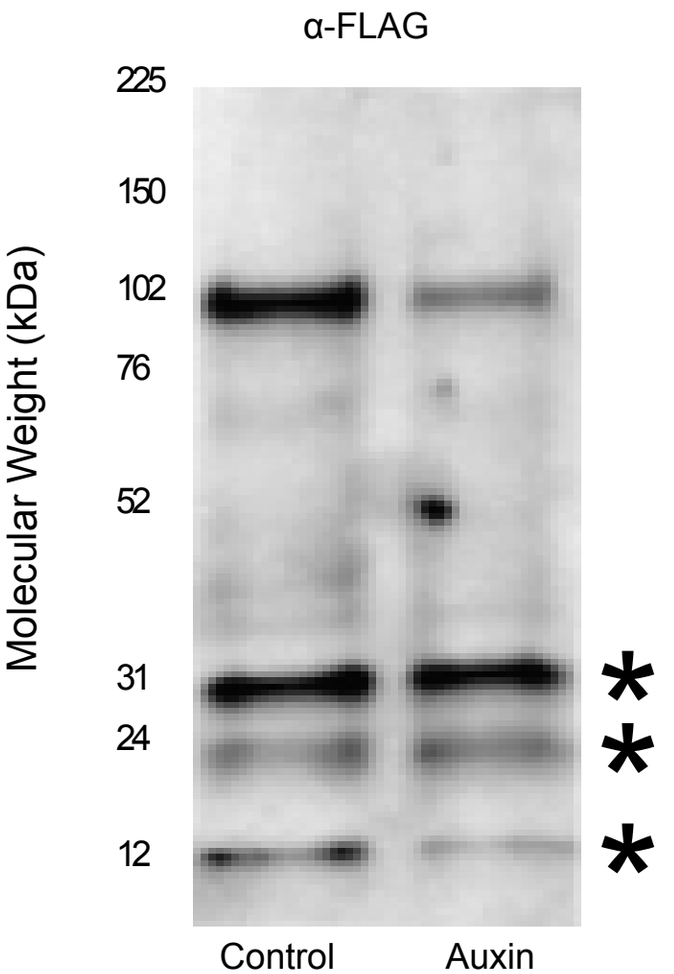

Fig. S2. Assessing NHR-23 depletion by western blot. Anti-FLAG immunoblot analyses as in Fig. 3 showing the entire blot. Stars indicate background bands previously reported (Ward, 2015).

A

Crossing Scheme					# Live Progeny	
Scheme Number	Male Genotype [crossed to *spe-8 (hc50); him-8 (e1489)*]	Life Stage of Male	Media	N	Mean (SD)	Median
1	None (self)	-	Control	10	0	0
2	*him-5 (e1490)*	L4	Control	9	185.6 (±116.5)	165
3	JDW92 *wrdSi19(mex-5p::TIR1), nhr-23(kry61(nhr-23::AID*-TEV-3xFLAG)); him-5(e1490)*	L4	Control	10	223.3 (±106.3)	232
4	JDW92 *wrdSi19(mex-5p::TIR1), nhr-23(kry61(nhr-23::AID*-TEV-3xFLAG)); him-5(e1490)*	L4	Auxin	14	32.9 (±56.7)	7.5
5	JDW92 *wrdSi19(mex-5p::TIR1), nhr-23(kry61(nhr-23::AID*-TEV-3xFLAG)); him-5(e1490)*	Young Adult	Auxin	10	0.4 (±0.8)	0

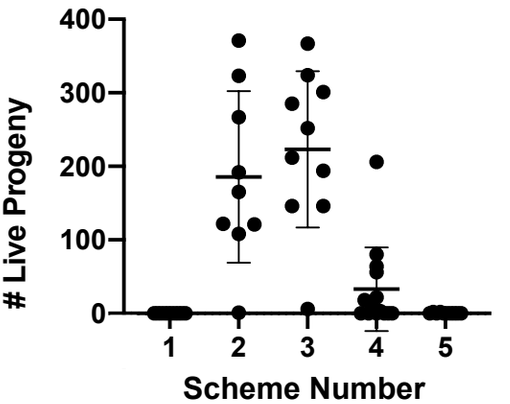

B

Fig. S3. Mating/Transactivation Assay. (A) Quantitation of live progeny produced from the indicated crosses to *spe-8(hc50); him-8(e1489)* hermaphrodites. Standard deviation (SD) is provided in the table. In the graph, the center horizontal lines for each crossing scheme represent mean and the whiskers represent standard deviation. (B) Image of JDW92 *wrdSi19[mex-5p::TIR1:F2A:mTagBFP2:tbb-2 3'UTR, I:-5.32], nhr-23(kry61(nhr-23::AID*::TEV::3xFLAG)) I; him-5(e1490) V* animals grown on auxin. The male in the image is engaging in mating behavior.

A

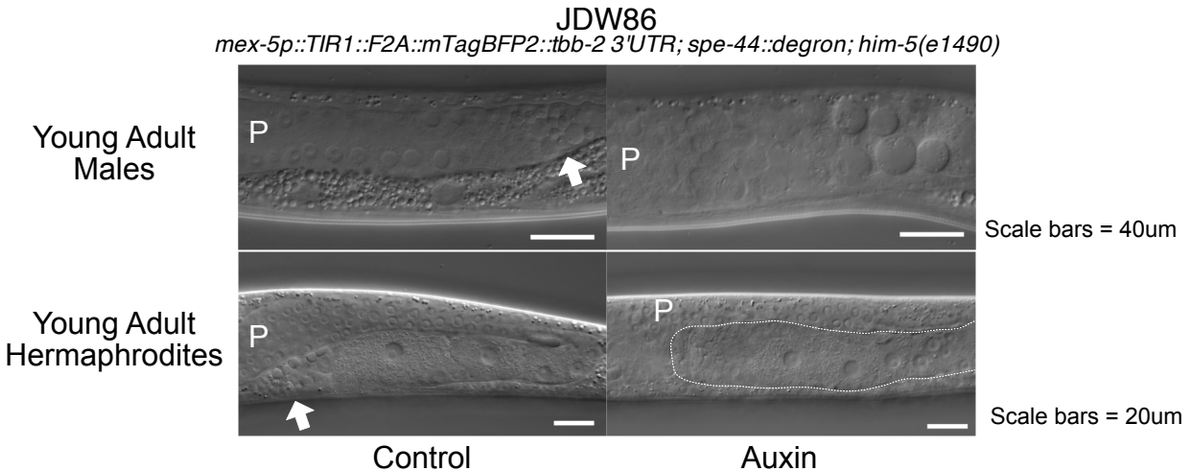

B

	Genotype	Media	N	Mean (SEM)	Median
N2	Wild-type	Control	12	273.5 (±11.4)	269
JDW101	*wrd20(spe-44::30xlinker::mScarlet::Lox511I::3xMyc)*	Control	12	264.8 (±8.6)	276
JDW86	*wrdSi15(mex-5p::TIR1:F2A:mTagBFP2:tbb-2 3'UTR); spe-44(fx110[spe-44::degron]); him-5(e1490)*	Control	14	126.6 (±9.5)	130
JDW86	*wrdSi15(mex-5p::TIR1:F2A:mTagBFP2:tbb-2 3'UTR); spe-44(fx110[spe-44::degron]); him-5(e1490)*	Auxin	12	0	0

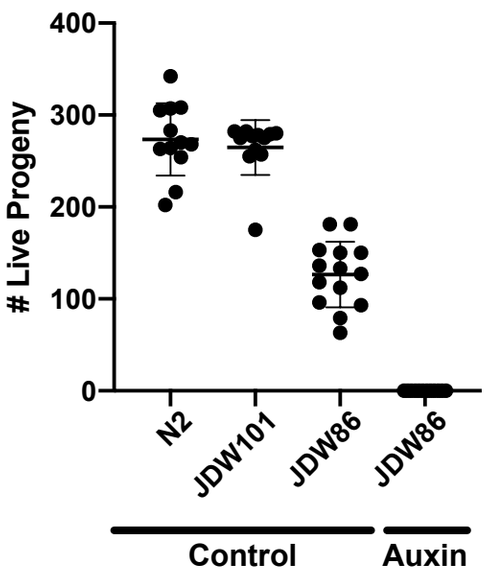

Fig. S4. Validation of *spe-44* alleles. (A) DIC images of JDW 86 *wrdSi15[mex-5p::TIR1:F2A:mTagBFP2:tbb-2 3'UTR]; spe-44(fx110[spe-44::AID*]); him-5(e1490)* young adult males and young adult hermaphrodites grown on control media or 4 mM auxin. The arrows point to examples of mature spermatids in control animal germlines. (B) Live progeny counts from animals of the indicated genotypes. Standard error of the mean (SEM) is provided in the table. In the graph, the center horizontal lines for each strain represent mean and the whiskers represent SEM.

Table S1. Plasmids used in this study		
Plasmid	**Parent plasmid or Reference**	**Notes**
pCZGY2747	Unpublished, gift from Zhiping Wang	*eft-3*p::*Cas9*; *U6*p::sgRNA vector targeting LGI site where ttTi4348 is inserted
pDD363	Dickinson *et al.*, 2018	LoxP-flanked SEC donor for the Sap Trap cloning system
pDD372	Dickinson *et al.*, 2018	Codon-optimized GFP donor for the Sap Trap cloning system
pDD379	Dickinson *et al.*, 2018	SapTrap destination vector for building combined sgRNA expression + repair template vectors, using the F+E sgRNA scaffold
pJW1254	Zhang *et al.*, 2015	*eft-3*p::Cas9; *U6p*::sgRNA (F+E) targeting *nhr-23* 3' end
pJW1357	Ashley *et al.*, 2020	*mex-5*p::TIR1:F2A:mTagBFP2 construct for knock-in at LGI site where ttTi4348 is inserted
pJW1598	Ashley *et al.*, 2020	linker::GFP^SEC^BioTag::AID*::3xFLAG vector for C-terminally tagging NHR-23
pJW1659	Ashley *et al.*, 2020	9 amino acid flexible linker::AID*-3xFLAG donor for NT slot in the Sap Trap cloning system
pJW1725	pDD379	repair template for C-terminally tagging NHR-23 generated by Sap Trap: linker::GFP^SEC^AID*::3xFLAG with *nhr-23* homology arms; *U6*p::*nhr-23* sgRNA (F+E)
pJW1776	pDONR221	*nhr-23* 5' homology arm for Sap Trap cloning (Sap sites in arm are silently mutated)
pJW1781	pDONR221	*nhr-23* 3' arm for Sap Trap cloning
pJW1816	Ashley *et al.*, 2020	30 amino acid flexible linker::mScarlet^SEC (Lox511I)^3xMyc multicassette donor for the Sap Trap cloning system
pJW1838	Ashley *et al.*, 2020	Sap Trap sgRNA vector, U6 promoter and 3'UTR from Calarco paper with F+E sgRNA modifications
pJW1872	pJW1838	*U6*::*sgRNA* targeting *spe-44* 3' end
pJW1876	Ashley *et al.*, 2020	repair template for C-terminally tagging SPE-44 generated by SapTrap:: 30 amino acid flexible linker::germ line optimized mScarlet^SEC (Lox511I)^3xMyc with *spe-44* homology arms
pJW258	pDONR221	*nhr-23* cDNA in Gateway entry vector
pMLS257	Schwartz *et al.*, 2016	Sap Trap repair template backbone lacking the *U6p::sgRNA* cassette
pMLS287	Schwartz *et al.*, 2016	SapTrap flexible 12 amino acid linker C-terminal connector donor plasmid

Table S2. Oligonucleotides used in this study

Click here to Download Table S2

Table S3. sgRNAs and repair oligos used for co-CRISPR in this study		
Name	**Purpose**	**Sequence**
dpy-10 sgRNA	Co-CRISPR to inactivate *fog-3*	taatacgactcactataggctaccataggcaccacgaggtttaagagctatgctggaaac
fog-3 sgRNA	Co-CRISPR to inactivate *fog-3*	taatacgactcactatagtagacgagaaatgtgagacggtttaagagctatgctggaa
dpy-10 (cn64) repair oligo	Co-CRISPR to inactivate *fog-3*	cacttgaacttcaatacggcaagatgagaatgactggaaaccgtaccgcatgcggtgcctatggtagcggagcttcacatggcttcagaccaacagcctat
fog-3 repair oligo	Co-CRISPR to inactivate *fog-3*	aggtcggcatatttggcgctgaacttggaaactacgaattctaaagtctcacatttctcgtctacctgggatgttcatca

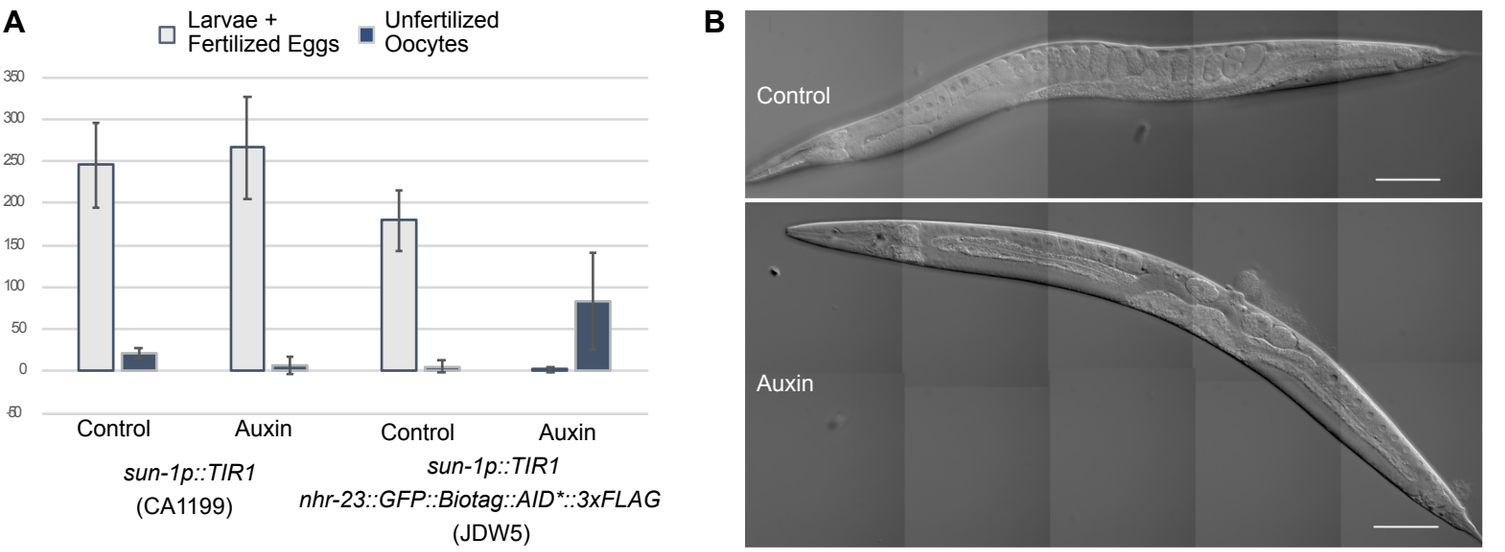

Fig. S1. NHR-23-depletion in worms expressing TIR1 from a *sun-1* promoter causes sterility similar to that observed when TIR1 is expressed from the *mex-5* promoter. (A) Combined count of L1 larvae/fertilized egg progeny or unfertilized oocyte from hermaphrodites grown from L1 onwards with or without 4 mM auxin. Error bars=standard deviation (n=12 for each condition) (B) Representative DIC images of L4 + 1 day *nhr-23::GFP::Biotag::AID*::3xFLAG; sun-1p::TIR1* hermaphrodites in the absence (top) or presence (bottom) of 4 mM auxin. Scale bars: 80 µm.

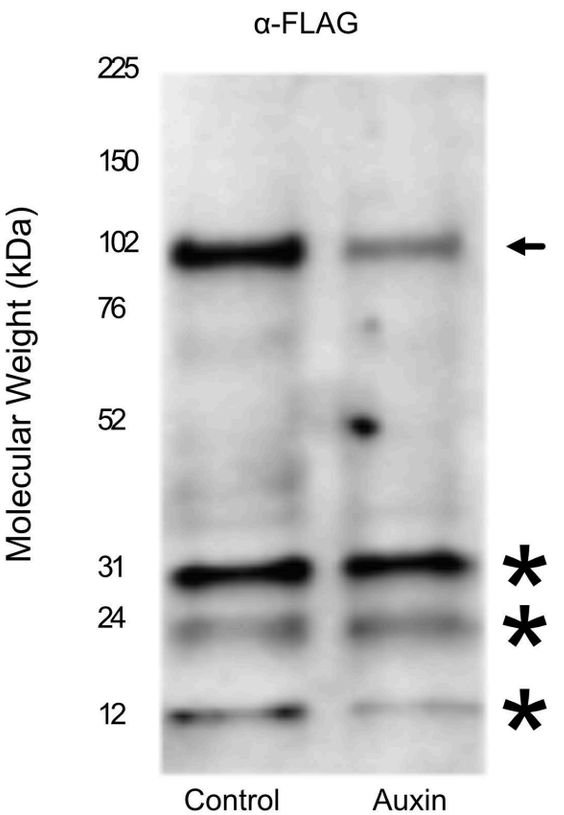

Fig. S2. Assessing NHR-23 depletion by western blot. Anti-FLAG immunoblot analyses as in Fig. 3 showing the entire blot. Arrow indicates NHR-23::GFP::AID*::3xFLAG band. Stars indicate background bands previously reported (Ward, 2015).

A

Crossing Scheme					# Live Progeny	
Scheme Number	Male Genotype [crossed to *spe-8 (hc50); him-8 (e1489)*]	Life Stage of Male	Media	N	Mean (SD)	Median
1	None (self)	-	Control	10	0	0
2	*him-5 (e1490)*	L4	Control	9	185.6 (±116.5)	165
3	JDW92 *wrdSi19(mex-5p::TIR1), nhr-23(kry61(nhr-23::AID*-TEV-3xFLAG)); him-5(e1490)*	L4	Control	10	223.3 (±106.3)	232
4	JDW92 *wrdSi19(mex-5p::TIR1), nhr-23(kry61(nhr-23::AID*-TEV-3xFLAG)); him-5(e1490)*	L4	Auxin	14	32.9 (±56.7)	7.5
5	JDW92 *wrdSi19(mex-5p::TIR1), nhr-23(kry61(nhr-23::AID*-TEV-3xFLAG)); him-5(e1490)*	Young Adult	Auxin	10	0.4 (±0.8)	0

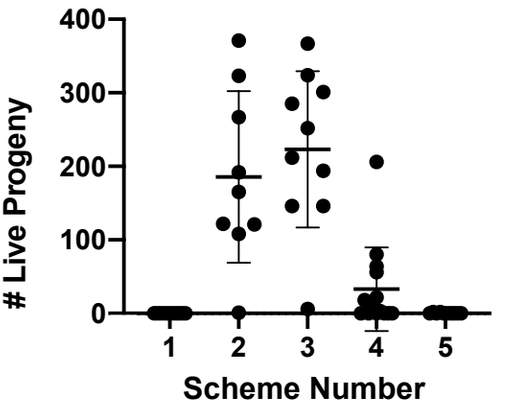

B

Fig. S3. Mating/Transactivation Assay. (A) Quantitation of live progeny produced from the indicated crosses to *spe-8(hc50); him-8(e1489)* hermaphrodites. Standard deviation (SD) is provided in the table. In the graph, the center horizontal lines for each crossing scheme represent mean and the whiskers represent standard deviation. (B) Image of JDW92 *wrdSi19[mex-5p::TIR1:F2A:mTagBFP2:tbb-2 3'UTR, I:-5.32], nhr-23(kry61(nhr-23::AID*::TEV::3xFLAG)) I; him-5(e1490) V* animals grown on auxin. The male in the image is engaging in mating behavior.

A

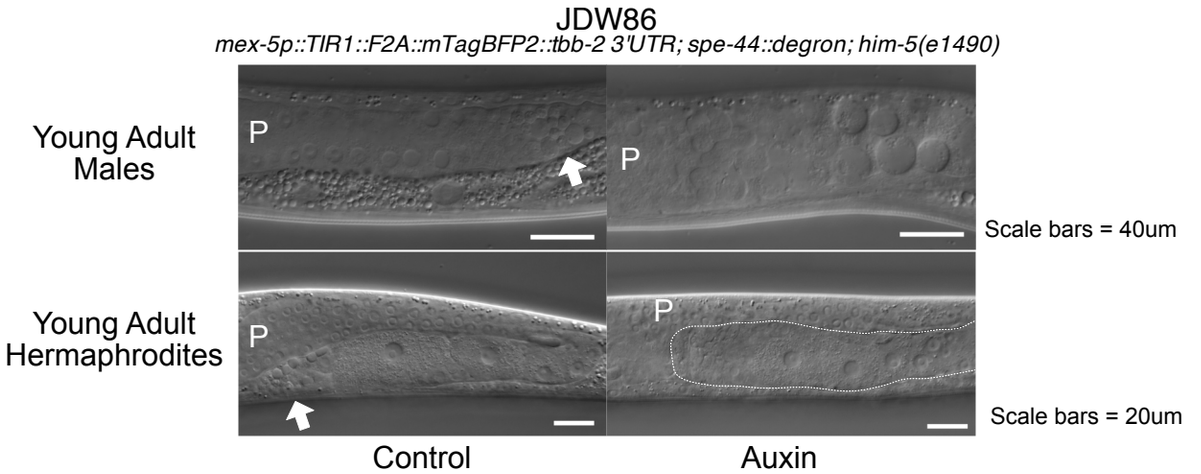

B

	Genotype	Media	N	Mean (SEM)	Median
N2	Wild-type	Control	12	273.5 (±11.4)	269
JDW101	*wrd20(spe-44::30xlinker::mScarlet::Lox511I::3xMyc)*	Control	12	264.8 (±8.6)	276
JDW86	*wrdSi15(mex-5p::TIR1:F2A:mTagBFP2:tbb-2 3'UTR); spe-44(fx110[spe-44::degron]); him-5(e1490)*	Control	14	126.6 (±9.5)	130
JDW86	*wrdSi15(mex-5p::TIR1:F2A:mTagBFP2:tbb-2 3'UTR); spe-44(fx110[spe-44::degron]); him-5(e1490)*	Auxin	12	0	0

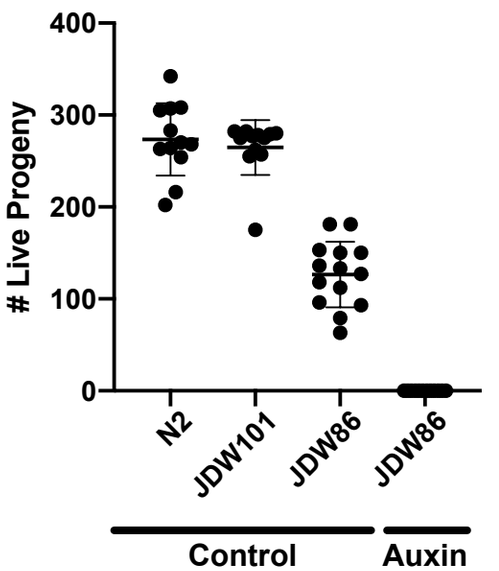

Fig. S4. Validation of *spe-44* alleles. (A) DIC images of JDW 86 *wrdSi15[mex-5p::TIR1:F2A:mTagBFP2:tbb-2 3'UTR]; spe-44(fx110[spe-44::AID*]); him-5(e1490)* young adult males and young adult hermaphrodites grown on control media or 4 mM auxin. The arrows point to examples of mature spermatids in control animal germlines. (B) Live progeny counts from animals of the indicated genotypes. Standard error of the mean (SEM) is provided in the table. In the graph, the center horizontal lines for each strain represent mean and the whiskers represent SEM.

Table S1. Plasmids used in this study		
Plasmid	**Parent plasmid or Reference**	**Notes**
pCZGY2747	Unpublished, gift from Zhiping Wang	*eft-3*p::*Cas9*; *U6*p::sgRNA vector targeting LGI site where ttTi4348 is inserted
pDD363	Dickinson *et al.*, 2018	LoxP-flanked SEC donor for the Sap Trap cloning system
pDD372	Dickinson *et al.*, 2018	Codon-optimized GFP donor for the Sap Trap cloning system
pDD379	Dickinson *et al.*, 2018	SapTrap destination vector for building combined sgRNA expression + repair template vectors, using the F+E sgRNA scaffold
pJW1254	Zhang *et al.*, 2015	*eft-3*p::Cas9; *U6p*::sgRNA (F+E) targeting *nhr-23* 3' end
pJW1357	Ashley *et al.*, 2020	*mex-5*p::TIR1:F2A:mTagBFP2 construct for knock-in at LGI site where ttTi4348 is inserted
pJW1598	Ashley *et al.*, 2020	linker::GFP^SEC^BioTag::AID*::3xFLAG vector for C-terminally tagging NHR-23
pJW1659	Ashley *et al.*, 2020	9 amino acid flexible linker::AID*-3xFLAG donor for NT slot in the Sap Trap cloning system
pJW1725	pDD379	repair template for C-terminally tagging NHR-23 generated by Sap Trap: linker::GFP^SEC^AID*::3xFLAG with *nhr-23* homology arms; *U6*p::*nhr-23* sgRNA (F+E)
pJW1776	pDONR221	*nhr-23* 5' homology arm for Sap Trap cloning (Sap sites in arm are silently mutated)
pJW1781	pDONR221	*nhr-23* 3' arm for Sap Trap cloning
pJW1816	Ashley *et al.*, 2020	30 amino acid flexible linker::mScarlet^SEC (Lox511I)^3xMyc multicassette donor for the Sap Trap cloning system
pJW1838	Ashley *et al.*, 2020	Sap Trap sgRNA vector, U6 promoter and 3'UTR from Calarco paper with F+E sgRNA modifications
pJW1872	pJW1838	*U6*::*sgRNA* targeting *spe-44* 3' end
pJW1876	Ashley *et al.*, 2020	repair template for C-terminally tagging SPE-44 generated by SapTrap:: 30 amino acid flexible linker::germ line optimized mScarlet^SEC (Lox511I)^3xMyc with *spe-44* homology arms
pJW258	pDONR221	*nhr-23* cDNA in Gateway entry vector
pMLS257	Schwartz *et al.*, 2016	Sap Trap repair template backbone lacking the *U6p::sgRNA* cassette
pMLS287	Schwartz *et al.*, 2016	SapTrap flexible 12 amino acid linker C-terminal connector donor plasmid

Table S2. Oligonucleotides used in this study

Click here to Download Table S2

Table S3. sgRNAs and repair oligos used for co-CRISPR in this study		
Name	**Purpose**	**Sequence**
dpy-10 sgRNA	Co-CRISPR to inactivate *fog-3*	taatacgactcactataggctaccataggcaccacgaggtttaagagctatgctggaaac
fog-3 sgRNA	Co-CRISPR to inactivate *fog-3*	taatacgactcactatagtagacgagaaatgtgagacggtttaagagctatgctggaa
dpy-10 (cn64) repair oligo	Co-CRISPR to inactivate *fog-3*	cacttgaacttcaatacggcaagatgagaatgactggaaaccgtaccgcatgcggtgcctatggtagcggagcttcacatggcttcagaccaacagcctat
fog-3 repair oligo	Co-CRISPR to inactivate *fog-3*	aggtcggcatatttggcgctgaacttggaaactacgaattctaaagtctcacatttctcgtctacctgggatgttcatca